NASA Technical Paper 1777

Leading-Edge Deflection Optimization for a Highly Swept Arrow-Wing Configuration

Paul L. Coe, Jr., Jarrett K. Huffman,
and James W. Fenbert

DECEMBER 1980

NASA

NASA Technical Paper 1777

Leading-Edge Deflection Optimization for a Highly Swept Arrow-Wing Configuration

Paul L. Coe, Jr., Jarrett K. Huffman,
and James W. Fenbert
Langley Research Center
Hampton, Virginia

National Aeronautics
and Space Administration

**Scientific and Technical
Information Branch**

1980

SUMMARY

An investigation has been conducted in the Langley High Speed 7- by 10-Foot Tunnel to determine the influence of an optimized leading-edge deflection on the low-speed aerodynamic performance of a configuration with a low-aspect-ratio, highly swept wing. Tests have also been conducted to determine the sensitivity of the lateral-stability derivative C_{l_β} to geometric anhedral.

The optimized leading-edge deflection was developed by aligning the leading edge with the incoming flow along the entire span. Owing to the spanwise variation of upwash, the resulting optimized leading edge was a smooth, continuously warped surface for which the deflection varied from 16° at the side of the body to 50° at the wing tip. For the particular configuration studied, levels of leading-edge suction on the order of 90 percent were achieved with the smooth, continuously warped leading-edge contour. Attempts to approximate this smooth contour by a series of discrete deflections of a multisegmented leading-edge system resulted in substantially increased drag. The increased drag, introduced by the surface discontinuities of the multisegmented system, markedly reduced the aerodynamic performance.

Deflecting the leading edge was found to provide a favorable reduction in the inherently high level of C_{l_β}. Comparison of experimental results with simple theoretical estimates of $\partial C_{l_\beta} / \partial C_L$ shows that excellent correlation exists for conditions of attached flow. Furthermore, the results of tests conducted to determine the sensitivity of C_{l_β} to geometric anhedral indicate values of $\partial C_{l_\beta} / \partial \Gamma$ which are in reasonable agreement with estimates provided by simple vortex-lattice theories.

INTRODUCTION

The National Aeronautics and Space Administration is currently investigating the aerodynamic characteristics of advanced aircraft concepts which are capable of cruising efficiently at supersonic speeds. The conceptual designs are representative of future generation commercial and military vehicles and incorporate wing sweeps on the order of 70° to 80° (e.g., refs. 1 and 2). Unfortunately, owing to the high wing sweeps, such configurations have generally exhibited unacceptable low-speed aerodynamic characteristics. The most significant of these unacceptable characteristics are deficiencies in low-speed performance and excessively high levels of effective dihedral (C_{l_β}). The present investigation is intended to yield fundamental information necessary to provide highly swept-wing designs with acceptable low-speed characteristics.

Previous low-speed studies with a configuration having the same wing geometry as the present model are reported in references 3 to 6. The present

study was specifically intended to: (1) provide an assessment of the aerodynamic performance benefits which could be achieved with a suitably optimized leading edge; and (2) determine the sensitivity of the lateral-stability derivative $\left(C_{l_\beta}\right)$ to geometric anhedral.

The tests were conducted in the Langley 7- by 10-Foot Tunnel over an angle-of-attack range from about -6° to 15° for sideslip angles of 0° and $\pm 5^\circ$. The tests were conducted at a Reynolds number (based on the wing mean aerodynamic chord) of about 2.8×10^6.

SYMBOLS

The longitudinal data are referred to the stability system of axes, and the lateral-directional data are referred to the body system of axes as illustrated in figure 1. The moment reference center for the tests was located at 59.166 percent of the reference wing mean aerodynamic chord. The reference wing area and reference mean aerodynamic chord are based on the wing planform which results from extending the inboard leading-edge sweep angle (74°) and the outboard trailing-edge sweep angle (41.457°) to the model center line. (See fig. 2.)

The dimensional quantities herein are given in both the International System of Units (SI) and the U.S. Customary Units.

A_{fus} fuselage cross-sectional area, m^2 (ft^2)

AR aspect ratio

b wing span, m (ft)

C_D drag coefficient, $\dfrac{\text{Drag}}{qS_{ref}}$

C_{D_i} induced drag coefficient

$C_{D_{min}}$ minimum drag coefficient

$C_{D_{sym}}$ drag coefficient of equivalent configuration without twist and camber at zero lift

C_L lift coefficient, $\dfrac{\text{Lift}}{qS_{ref}}$

C_l rolling-moment, $\dfrac{\text{Rolling moment}}{qS_{ref}b}$

C_m pitching-moment coefficient, $\frac{\text{Pitching moment}}{qS_{ref}\bar{c}}$

C_n yawing-moment coefficient, $\frac{\text{Yawing moment}}{qS_{ref}b}$

C_Y side-force coefficient, $\frac{\text{Side force}}{qS_{ref}}$

$\bar{c}$ reference mean aerodynamic chord, m (ft)

q free-stream dynamic pressure, Pa (lbf/ft^2)

S leading-edge suction parameter

S_{ref} reference wing area, m^2 (ft^2)

X,Y,Z body axes system

x,y,z body axes coordinates

x_{fus} fuselage body station, origin at nose, positive rearward, m (ft)

α angle of attack, deg

β angle of sideslip, deg

Γ increment in geometric anhedral, relative to the basic wing geometry, at span station y, deg

Γ_1,Γ_2 increment in geometric anhedral at span stations y_1 and y_2, respectively, deg (see fig. 2(b))

$\delta_{L.E.}$ leading-edge deflection, positive when leading edge is down, deg

ε upwash angle, deg

ξ X-Y projection of the included angle between the local flow direction at the leading edge and a ray normal to the leading-edge hinge line, deg (see fig. 1)

Derivatives:

C_{L_α} $= \partial C_L/\delta\alpha$, per deg

C_{l_β} $= \partial C_l/\delta\beta$, per deg

C_{n_β} = $\partial C_n/\delta\beta$, per deg

C_{Y_β} = $\partial C_Y/\delta\beta$, per deg

MODEL

The principal dimensional characteristics of the model used in the present study are listed in table I and shown in figures 2 and 3. In addition, a listing of the computer cards required for a numerical model is given in table II. The format for the listing provided in table II is described in reference 7. A photograph of the model in the Langley 7- by 10-Foot Tunnel is presented in figure 4.

Previous studies with configurations having the same wing geometry as the present model are reported in references 3 to 6. The present study was intended to address generic problems associated with highly swept wings; consequently, the model did not incorporate either nacelles or an aft fuselage. The model did, however, incorporate a multisegmented leading edge which permitted continuously variable deflections from 0° to 60° about the 70.688° swept hinge line. (See fig. 2.) This particular hinge line was selected to allow a direct comparison with results from reference 5. The model further incorporated anhedral breaks at span stations $\frac{y}{b/2} = 0.234$ and 0.736 which permitted the inclusion of additional geometric anhedral.

TESTS AND CORRECTIONS

The investigation was conducted in the Langley 7- by 10-Foot Tunnel. (See ref. 8 for a description of the tunnel.) Forces and moments were measured with a standard six-component strain-gage balance mounted internal to the model. The tests were conducted at a dynamic pressure of 1436.4 Pa (30 lbf/ft^2). This value of dynamic pressure resulted in a Reynolds number (based on the wing mean aerodynamic chord) of 2.8×10^6 at a corresponding Mach number of 0.14. The angle of attack ranged from about -6° to 15° for sideslip angles of 0° and $\pm5^\circ$. Both angle of attack and sideslip have been corrected for the effect of sting and balance bending under aerodynamic load.

The data have been corrected for jet-boundary and blockage effects using the methods outlined in references 9 and 10, respectively. Balance chamber pressure and model base pressure were measured and the drag measurements adjusted to correspond to conditions of free-stream static pressure acting over the base of the model.

In accordance with the method of reference 11, 0.16 cm (0.0625 in.) wide transition strips of No. 70 carborundum grains were placed 3.81 cm (1.5 in.) aft of the leading edges of the wing and outboard vertical tails. Similarly, No. 80 carborundum grains were placed 3.81 cm (1.5 in.) aft of the model nose.

PRESENTATION OF RESULTS

A simplified analysis of the effect of geometric anhedral on C_{l_β} is presented in appendix A. A data supplement containing a run schedule and tabular listing of data is provided in appendix B. The results and discussion are presented in accordance with the following outline:

RESULTS AND DISCUSSION

The present study was intended to address generic problems associated with highly swept wings; therefore, the model did not incorporate either nacelles or an aft fuselage. In order to provide some insight into the possible effects such configuration components may have on absolute quantities, suitable comparisons are made (where possible) with data obtained for a model which had the same wing geometry, but included both underwing nacelles and an aft fuselage (see ref. 5). It should be noted that, in addition to the nacelle and aft fuselage differences, the model of reference 5 incorporated a fuselage with a different cross-sectional area distribution (see fig. 3). Since the fuselages of both the present model and the model of reference 5 utilized circular cross sections and had the same centroidal axis, the difference in cross-sectional area results in a difference in wing-body intersection.

Longitudinal Aerodynamic Characteristics

Configuration with undeflected leading edge.- Figure 5 presents the longitudinal aerodynamic characteristics for the present configuration with undeflected leading edges ($\delta_{L.E.} = 0$). Also presented for purposes of comparison are corresponding data for the complete configuration reported in reference 5. As can be seen, the data exhibit identical trends. The study of reference 5, in which smoke-flow visualization was used, has indicated that for angles of attack from about 2° to 4° the flow over the main wing panel remains well attached; however, the existence of a tightly wound vortex which formed close to the surface along the leading edge of the outboard wing panel has been observed. As might be anticipated, this tightly wound vortex is found to be accompanied by a small increase in longitudinal stability. At $\alpha > 4^\circ$, the data indicate the existence of a vortex-lift increment and a corresponding pitch-up tendency. This result is attributed to the simultaneous formation of classical wing-apex vortices and to the separation of the tightly wound vortex from the outboard wing panel. (See ref. 5.)

The data of reference 5 exhibit trends which are identical to those of the present model. However, configuration differences result in differences

in the quantitative values. Obviously, the lower value of drag exhibited by the present model results from the reduced skin-friction and interference drag associated with the omission of the aft fuselage and underwing nacelles. The reduction in pitching moment of the present model is attributed to the omission of the down-loaded aft fuselage (see ref. 5). The difference in level of vortex lift for the two configurations is not well understood. However, this difference probably arises from the difference in the wing-body intersection which may, in turn, affect the formation of the wing-apex vortices.

Figure 6 presents theoretical results obtained using a vortex-lattice representation for the isolated twisted and cambered wing of the present model. In addition to the standard potential-flow calculations, this particular vortex-lattice method (see ref. 12) also permits calculation of the aerodynamic characteristics for conditions with leading-edge vortex flows. This is accomplished by incorporating the leading-edge suction analogy developed in reference 13. The results of figure 6 illustrate that the predicted aerodynamic characteristics for conditions of leading-edge vortex flows, are markedly different from those predicted for attached flow conditions. In particular, consideration of the theoretical drag polars (obtained by adding the value of $C_{D_{sym}} = 0.0096$ to the predicted induced drag) indicates that the particular wing geometry, which was designed for attached flow conditions, would have significantly degraded performance for conditions with separated leading-edge vortices.

The vortex-lattice theoretical method used to obtain the results presented in figure 6 does not predict the onset condition or the physical spanwise location of the separated vortex flow; therefore, no one of the theoretical curves is representative over the entire angle-of-attack range considered. Figure 7 presents an adjusted theoretical result obtained by shifting portions of the appropriate curves of figure 6 in an attempt to more closely represent the results for the observed physical flow condition. As can be seen, reasonable agreement exists between this adjusted theoretical result and the experimental result. However, it is recognized that such adjusted theoretical results can only be achieved after the physical flow characteristics have been identified, and hence, may be of limited value.

Effect of wing leading-edge deflection.- Figure 8 presents the longitudinal aerodynamic characteristics for the configuration with a uniform 30° deflection of the entire leading edge (see fig. 2). As has been shown in reference 5, this leading-edge deflection results in fairly well attached flow for angles of attack from about 0° to 8°. For angles of attack greater than 8°, smoke-flow observations showed the onset of a classical leading-edge vortex separation originating at about the midpoint of the wing semispan. It should also be noted that at very low angles of attack ($\alpha < 0^{\circ}$), deflecting the leading edges apparently results in flow separation on the lower wing surfaces as evidenced by the nonlinearity in C_L versus α. Figure 8 also presents the longitudinal aerodynamic data from reference 5 for the comparable ($\delta_{L.E.} = 30^{\circ}$) condition. As can be seen, the differences in data for the present tests and reference 5 are generally similar to those previously discussed for the $\delta_{L.E.} = 0^{\circ}$ condition. As expected, with the leading edges deflected to suppress the leading-edge vortices, excellent agreement in C_L versus α is obtained over the angle-of-attack range tested.

Figure 9 provides a comparison of the data for the conditions of $\delta_{L.E.} = 0^{o}$ and 30^{o}. As has been noted in reference 5, deflecting the wing leading edges to suppress the vortex flow reduces the undesirable vortex induced pitch-up tendency and also reduces the vortex related drag. In order to permit a quantitative evaluation of the performance improvement achieved by leading-edge deflection, figure 9 also presents the conventional theoretical drag polars corresponding to the conditions of: (1) minimum induced drag (100-percent leading-edge suction) and (2) full leading-edge separation (0-percent leading-edge suction). These drag polars are defined for condition (1) as

$$C_D = C_{D_{sym}} + C_L^2/\pi AR \tag{1}$$

and for condition (2) as

$$C_D = C_{D_{sym}} + C_L \tan \left(C_L/C_{L_\alpha}\right) \tag{2}$$

It should be noted that equations (1) and (2) are valid only for symmetric wings with no twist or camber and are presented herein solely to permit the aerodynamic performance (achieved by the various leading-edge treatments) to be quantified. This is accomplished by introducing the standard leading-edge suction parameter S (see ref. 14 for a comprehensive discussion of leading-edge suction) defined as

$$S = \frac{C_D - \left[C_{D_{sym}} + C_L \tan \left(C_L/C_{L_\alpha}\right)\right]}{C_L^2/\pi AR - C_L \tan \left(C_L/C_{L_\alpha}\right)} \tag{3}$$

It should be noted that in equations (2) and (3) the quantity $C_L \tan \left(C_L/C_{L_\alpha}\right)$ has been used in place of the more customary $C_L \tan \alpha$. (See ref. 14.) This present notation has been introduced to insure a common basis for comparison of leading-edge suction for the various leading-edge treatments. The value of $C_{D_{sym}}$ has been estimated for the present model tests using the relationship

$$C_{D_{sym}} = C_{D_{min}} - \frac{C_L^2 \left|C_{D_{min}}\right.}{\pi AR} \tag{4}$$

Evaluation of equation (4) yields $C_{D_{sym}} = 0.0096$. The value of C_{L_α} has been determined experimentally (for the linear region of C_L versus α) to be 0.037 which is in agreement with theoretical results.

Figure 10 presents values of leading-edge suction calculated from the data of figure 9. As can be seen, the uniform 30° deflection results in substantially increased values relative to the $\delta_{L.E.} = 0^{\circ}$ condition. This result is similar to the results presented in reference 5, wherein this uniform 30° deflection was initially considered. As pointed out in reference 5, the uniform 30° deflection does not represent an optimum condition. In fact, the uniform 30° deflection is considered to be overdeflected in the apex region while being underdeflected further outboard. This situation developed because the leading-edge system tested in reference 5 was limited to four segments, and attempts to optimize the leading-edge deflection by aligning the leading edge with the local upwash (as will be discussed) resulted in large discontinuities in contour. These large discontinuities were found to result in quite pronounced regions of separated flow, which substantially degraded the performance. Consequently, the uniform 30° deflection was considered an appropriate compromise.

In as much as the present configuration employed a twelve-segmented leading edge (which permitted a more reasonable approximation of a continuously warped surface), an attempt was made to optimize the spanwise variation of leading-edge deflection. The optimal leading edge is considered herein as one in which the leading edge is aligned with the upwash along the entire span. Since $\alpha = 10^{\circ}$ is representative of the angle-of-attack condition for low-speed operations, attempts were made to obtain attached flow for angles of attack at least up to this condition.

Figure 11 presents the theoretical spanwise variation of upwash ε obtained with a vortex-lattice computational model at an angle of attack of 10° (see refs. 5 and 15). In general, for a swept hinge line the angular deflection required to align the leading edge with an upwash angle ε would be defined by the standard relationship of sweep theory

$$\delta_{L.E.} = \tan^{-1}\left[\frac{\tan \varepsilon}{\cos \xi}\right] \tag{5}$$

However, previous smoke-flow studies (see ref. 5) have shown that the incoming flow is approximately perpendicular to the hinge line ($\xi = 0^{\circ}$), and therefore, equation (5) yields the simple result that $\delta_{L.E.} = \varepsilon$.

With the model at $\alpha = 10^{\circ}$ and the leading edge deflected to approximate the upwash schedule of figure 11, observations of wool surface tufts revealed flow separation originating outboard of $\frac{y}{b/2} = 0.5$. This result appears to be attributable to the fairly sharp corner introduced by rather high deflection about the simple hinge line. Accordingly, the leading-edge deflection was reduced until a condition was reached wherein further reductions resulted in classical leading-edge vortex separation. The multisegmented leading edge was then faired and smoothed to eliminate leading-edge discontinuities. The spanwise variation of leading-edge deflection, as developed above, is compared in

figure 12 with the theoretical upwash. The leading-edge deflection schedule is seen to define a continuously warped surface which varies from 16° inboard to 50° outboard. This leading-edge geometry will hereinafter be designated as $\delta_{L.E.} = 16^{\circ}\text{-}50^{\circ}$.

Figure 13 presents the longitudinal aerodynamic characteristics obtained with $\delta_{L.E.} = 16^{\circ}\text{-}50^{\circ}$, while figure 14 presents a comparison of these data with the previously discussed results for the $\delta_{L.E.} = 0^{\circ}$ and 30° conditions. As can be seen, the data for $\delta_{L.E.} = 16^{\circ}\text{-}50^{\circ}$ indicate attached flow conditions for angles of attack from about 0° to 10°. At angles of attack above 10°, vortex separation was observed to originate along the leading edge outboard of $\frac{y}{b/2} = 0.5$. The occurrence of this leading-edge separation is seen to be consistent with the slight pitch-up characteristic exhibited by the data of figure 13. Consideration of the drag polars of figure 14 indicates that $\delta_{L.E.} = 16^{\circ}\text{-}50^{\circ}$ provides superior aerodynamic performance relative to the other conditions studied. This point is quantified by considering the leading-edge suction parameter obtained for the above continuously warped leading-edge geometry ($\delta_{L.E.} = 16^{\circ}\text{-}50^{\circ}$) presented in figure 15. As has been seen, $\delta_{L.E.} = 16^{\circ}\text{-}50^{\circ}$ results in a substantial improvement. In particular, $\delta_{L.E.} = 16^{\circ}\text{-}50^{\circ}$ is seen to achieve values of suction on the order of 90 percent at representative second segment climb conditions (i.e., $C_L \approx 0.3$). However, at higher values of C_L (corresponding to higher angles of attack) the level of leading-edge suction is substantially reduced for all leading edge geometries tested. It should be noted that the model tested did not employ a trailing edge flap system, which would permit equivalent values of C_L to be achieved at lower angles of attack. Therefore, owing to the adverse effect of increasing α on flow attachment, it would be anticipated that the use of a trailing edge flap system would provide improved drag polars (as shown by fig. 13(c) of ref. 5). Consequently the values of S presented herein for the high lift condition are regarded as conservative.

The effect of Reynolds number on the leading-edge suction parameter has been discussed in reference 14. The results presented therein indicate that increasing the Reynolds number from the low values of the present tests to actual flight values will result in only modest increases in S for the separated flow condition (e.g., the condition discussed herein with $\delta_{L.E.} = 0^{\circ}$). However, for attached flow conditions (as achieved with $\delta_{L.E.} = 16^{\circ}\text{-}50^{\circ}$) increasing Reynolds number results in pronounced increases in S. Based on these results, it would appear that the level of S achieved with the attached flow deflection $\delta_{L.E.} = 16^{\circ}\text{-}50^{\circ}$ is conservative.

It is recognized that while the continuously warped leading edge would provide marked improvements in low-speed aerodynamic performance, the mechanical complexity required to generate this smooth contour from the high-speed cruise shape may limit its practical application. For this reason, tests were conducted in which $\delta_{L.E.} = 16^{\circ}\text{-}50^{\circ}$ was preserved but the fairing between the adjacent segments of the multisegmented system removed. Figure 16 presents a comparison of the longitudinal data obtained with $\delta_{L.E.} = 16^{\circ}\text{-}50^{\circ}$ for both faired and unfaired conditions. As can be seen, the impact of removing the leading-edge fairings is largely limited to an increase in drag. This result

correlates well with observations made of wool tufts during the limted flow visualization portion of the tests. Although no large regions of separation could be attributed to the removal of the segment fairings, the tufts were observed to be slightly more unsteady, thereby indicating localized regions of separation. Consideration of the leading-edge suction parameter presented in figure 17 shows that $\delta_{L.E.} = 16^{o}$-50^{o} exhibits levels of S which are below those values achieved with the simple uniform 30^{o} deflection, thereby indicating the desirability of maintaining continuous leading-edge contour.

Lateral-Directional Characteristics

Configuration with undeflected leading edge.- Figure 18 presents the lateral-directional stability derivatives for the present configuration with undeflected leading edges. Also presented in figure 18 are corresponding results from reference 5 which, as previously mentioned, were obtained with a model which had the same wing geometry but incorporated a different fuselage and included under-wing nacelles. As can be seen from figure 18, both configurations exhibit neutrally stable values of static directional stability C_{n_β} for angles of attack up to about 4^{o}. For angles of attack greater than 4^{o} (corresponding to the angle of attack for which the wing-apex vortices are first evident), the configuration exhibits a marked increase in C_{n_β}. This phenomenon has been observed previously (see ref. 5) and has been attributed to the interaction of the wing-apex vortices with the forward portion of the configuration.

The data of figure 18 also show that both configurations exhibit high levels of effective dihedral C_{l_β} at nominal approach conditions of $\alpha = 8^{o}$ to 10^{o}, as would be expected for the low-aspect-ratio wing. References 16 and 17 have shown that these high levels of C_{l_β} typically result in Dutch roll instabilities and reversals in pilot-commanded roll rates. The analysis of reference 4 has also shown that, because of limited lateral-control capabilities (typical of low-aspect-ratio wings) the high values of C_{l_β} would necessitate excessive approach speeds to meet currently accepted cross-wind landing requirements.

It is interesting to note that although both the present configuration and the configuration of reference 5 exhibit about the same slope of C_{l_β} versus α, the magnitude of C_{l_β} for the present configuration is reduced for positive angles of attack. This reduction in C_{l_β} is believed to be due to the omission of the under-wing nacelles and to a difference in the aft wing-body intersection (e.g., ref. 18).

Effect of wing leading-edge deflection.- Figure 19 presents the lateral-directional stability derivatives for the configuration with $\delta_{L.E.} = 0^{o}$, 30^{o},

and 16°-50°. As can be seen by comparison of the results presented, both of the deflected leading-edge geometries resulted in a reduction in C_{n_β}. The reduction in C_{n_β} at low angles of attack is simply due to the deflected leading edge providing an increased vertical area forward of the moment reference center. At higher angles of attack, the dramatic reduction in C_{n_β} is, of course, associated with the suppression of the wing-apex vortices. Although this reduction in C_{n_β} at high angles of attack may appear to be adverse, previous studies (see ref. 19) have shown that positive increments in C_{n_β}, when originating forward of the center of gravity (as is the case considered herein), are accompanied by undesirable reductions in damping in yaw. For the present configuration the influence of leading-edge deflection on damping in yaw is undetermined, and additional tests are required to determine the effect of leading-edge deflection on dynamic stability characteristics.

The data of figure 19 also indicate that deflecting the leading edge yields a favorable increment in C_{l_β}. This result is primarily due to the simple increase in geometric anhedral which accompanies the leading-edge deflections. Figure 20 presents these same data as the variation of C_{l_β} with respect to C_L for the various leading-edge deflections. Noted on the figures are the regions of separated and attached flow as discussed in connection with figures 5, 8, and 13. Analysis of the results shows that, for the conditions under which attached flow exists, positive increments in C_{l_β} of 0.00016 and 0.00022 are obtained (relative to $\delta_{L.E.} = 0°$) for $\delta_{L.E.} = 30°$ and 16°-50°, respectively.

It should be noted that for conditions of attached flow, $\partial C_{l_\beta}/\partial C_L$ is found to be independent of leading-edge geometry and has a value of -0.0058. This value of $\partial C_{l_\beta}/\partial C_L$ is in excellent agreement with the value of -0.0061 obtained from the expression

$$\partial C_{l_\beta}/\partial C_L = \frac{2}{3} \times \frac{1}{AR} \times \frac{2\pi}{360} \tag{6}$$

which is developed in reference 20. The break in the slope of C_{l_β} versus C_L is a result of flow separation. Although it is not clearly understood, apparently the nature of the leading-edge separation greatly influences the manner in which the break in slope occurs. In as much as a properly designed configuration would be intended to operate with attached flow, the values of C_{l_β} for conditions of separated flow may be misleading. Extrapolation of the attached flow results to higher lift coefficients (as could be achieved with a simple trailing-edge flap system) shows that with the leading-edge geometries

studied the configuration would exhibit values of C_{l_β} of about -0.003 at a nominal approach lift coefficient of 0.6.

Effect of geometric anhedral.- The results of the preceding section indicates that, as expected, high values of C_{l_β} are inherent to the low-aspect-ratio highly swept wing. Consequently, tests were conducted in order to determine the sensitivity of C_{l_β} to additional geometric anhedral and to correlate these results with existing theory. These tests were conducted with the geometric anhedral increased at span stations $\frac{y}{b/2} = 0.234$ and 0.736 (see fig. 2). The leading-edge geometry for the configuration during this phase of the study was limited to the continuously warped $\delta_{L.E.} = 16^o\text{-}50^o$ condition, which was previously found to exhibit superior longitudinal performance. Examination of the tabulated data (presented in the data supplement at the end of this report) for the various anhedral angles tested shows that the longitudinal variables were not influenced by anhedral. The data further show that the geometric anhedral does not have any significant effect on the directional stability characteristics. Consequently, the discussion is limited to a consideration of the influence of geometric anhedral on C_{l_β}.

Figures 21 and 22 present the variation of C_{l_β} with C_L for the various anhedral angle combinations tested. From theoretical considerations, it would be expected that the values of $\partial C_{l_\beta}/\partial\Gamma$ (as determined by cross plotting the data of fig. 21) would be constant for attached flow conditions. However, analysis of the data of figure 21 shows that $\partial C_{l_\beta}/\partial\Gamma$ increases with increasing lift coefficient. To determine the additive nature of the experimental results for C_{l_β} versus C_L, a selected combination of $\Gamma_1 = 4^o$ and $\Gamma_2 = 11^o$ was tested. The experimental results (see fig. 22) are seen to compare well with results obtained by adding the experimentally determined incremental values of C_{l_β} presented in figure 21.

Figure 23 presents the theoretical variation of $\partial C_{l_\beta}/\partial\Gamma$ as a function of the corresponding nondimensional semispan location. The theoretical results were obtained with a vortex-lattice computational model which is based on the theory of reference 15. The range of experimental results for $\partial C_{l_\beta}/\partial\Gamma$, evaluated from figure 21 at $C_L = 0.2$ and 0.4 are presented for comparison. It is noted that although the experimental values of $\partial C_{l_\beta}/\partial\Gamma$ have been shown to increase with increasing C_L, they are in reasonable agreement with the theoretical results. Furthermore, both the vortex-lattice theoretical results and

the experimental results are seen to be in agreement with the approximate values of $\partial C_{l_\beta}/\partial \Gamma$ obtained using the simple design chart procedure contained in reference 21.

The results presented in figure 23 indicate that quite substantial reductions in C_{l_β} may be achieved by introducing geometric anhedral at inboard span locations. However, it should be recognized that a detailed configuration study is required to determine the most effective means of incorporating such additional anhedral.

As an illustration, the simplified analysis presented in appendix A considers the case wherein anhedral is added at an inboard span location. The analysis assumes that the wing-tip clearance remains unchanged as would be required for the case where the landing gear length was held constant. Obviously, under these conditions, adding geometric anhedral at inboard locations necessitates the addition of dihedral at outboard locations. The results presented in appendix A show that for these conditions, the net resulting improvement in C_{l_β} is negligible.

SUMMARY OF RESULTS

The results of a study to determine the influence of optimized leading-edge deflection and geometric anhedral on the low-speed performance and lateral stability of configurations with highly swept wings may be summarized as follows:

1. Leading-edge deflection is effective in suppressing the formation of wing-apex vortices and promoting attached flow conditions.

2. Due to the spanwise variation of upwash, the optimal leading-edge deflection is a smooth, continuously warped surface. For the particular configuration studied, levels of leading-edge suction in excess of 90 percent are achieved with a smooth, continuously varying leading-edge deflection of 16° at the side of the body and increasing to 50° at the wing tip.

3. Small discontinuities in surface contour, introduced in an attempt to approximate the smooth continuously warped leading edge with a series of discrete deflections of a multisegmented leading-edge system, resulted in large increments in drag (apparently due to flow separation) and corresponding large reductions in the leading-edge suction parameter.

4. A uniform leading-edge deflection of 30° (representing an average value of the continuously warped leading-edge deflection) provided higher values of the leading-edge suction parameter than provided by the discrete multisegmented system. This result is apparently due to the elimination of the small surface discontinuities introduced by deflecting the individual segments through different angles.

5. Deflecting the entire leading edge to achieve attached flow is found to provide a favorable reduction in the inherently high level of C_{l_β} which is associated with the low-aspect-ratio highly swept wing.

6. The theoretical value of $\partial C_{l_\beta}/\partial C_L$ is found to be in excellent agreement with experimental results for conditions where attached flow exists.

7. The inclusion of additional geometric anhedral to reduce the high levels of C_{l_β} is found to yield values of $\partial C_{l_\beta}/\partial \Gamma$ which are in reasonable agreement with theoretical estimates.

Langley Research Center
National Aeronautics and Space Administration
Hampton, VA 23665
November 25, 1980

TABLE I.- GEOMETRIC CHARACTERISTICS OF MODEL

Wing:	
Aspect ratio	1.904
Reference area, m^2 (ft^2)	0.834 (8.972)
Gross area, m^2 (ft^2)	0.919 (9.889)
Span, m (ft)	1.260 (4.133)
Root chord, m (ft)	1.674 (5.492)
Tip chord, m (ft)	0.161 (0.529)
Reference mean aerodynamic chord, m (ft)	0.880 (2.887)
Gross mean aerodynamic chord, m (ft)	1.038 (3.406)
Leading-edge sweep, deg	
At body station 0.388 m (1.272 ft)	74.0
At body station 1.427 m (4.683 ft)	70.5
At body station 1.886 m (6.185 ft)	60.0
Vertical fin (each):	
Span, m (ft)	0.107 (0.350)
Root chord, m (ft)	0.326 (1.069)
Tip chord, m (ft)	0.048 (0.158)
Leading-edge sweep, deg	73.4

TABLE II.- NUMERICAL MODEL OF CONFIGURATION

(a) SI Units. All dimensions are in centimeters

```
  1  1  1  1  1  1    13 24  4 25  7 22  9 28  9 27  8  2 10  2 10  1 10
8335.35                                                                  REFA
0.      .125   .25    .5     .75    1.0    1.5    2.5    5.0    10.      XAF 10
15.     20.    30.    40.    50.    60.    65.    70.    75.    80.      XAF 20
85.     90.    95.   100.                                               XAF
 56.596  5.111 -3.722149.382                                            WORG1
 60.302  6.174 -4.691145.744                                            WORG 2
 69.065  8.687 -6.209136.931                                            WORG  2A
 81.836 12.349 -7.590124.084                                            WORG 3
103.367 18.523 -9.144102.425                                            WORG4
112.115 21.031 -9.711 93.625                                            WORG 5
124.899 24.697-10.488 81.832                                            WORG 6
142.728 29.809-11.220 65.385                                            WORG7
156.394 34.564-11.659 53.003                                            WORG 8
163.527 37.046-11.951 48.143                                            WORG9
188.458 45.720-12.875 31.153                                            WORG10
188.458 45.721-12.875 31.153                                            WORG11
218.359 62.992-14.630 16.496                                            WORG 12
  0.000   .001   .001  0.000  -.001  -.002  -.007  -.024  -.119  -.475  TZ   1.1
 -1.015 -1.673 -3.164 -4.755 -6.346 -7.800 -8.431 -9.025 -9.583-10.095  TZ   1.2
-10.570-11.000-11.375-11.704                                            TZ   1.3
  0.000   .001   .002   .003   .003   .003   .001  -.005  -.041  -.311  TZ   2.1
  -.750 -1.308 -2.579 -4.005 -5.468 -6.767 -7.343 -7.910 -8.449 -8.989  TZ   2.2
 -9.464 -9.903-10.269-10.580                                            TZ   2.3
  0.000   .003   .006   .012   .018   .023   .034   .053   .082   .064  TZ  2A.1
  -.393  -.805 -1.801 -2.917 -4.069 -5.176 -5.678 -6.190 -6.684 -7.151  TZ  2A.2
 -7.590 -7.992 -8.358 -8.678                                            TZ  2A.3
  0.000   .005   .009   .018   .027   .036   .050   .078   .129   .052  TZ   3.1
  -.158  -.438 -1.133 -1.933 -2.784 -3.648 -4.074 -4.493 -4.904 -5.301  TZ   3.2
 -5.684 -6.051 -6.398 -6.724                                            TZ   3.3
  0.000   .005   .009   .020   .031   .042   .064   .101   .190   .226  TZ   4.1
   .157   .031  -.341  -.810 -1.342 -1.909 -2.199 -2.492 -2.784 -3.075  TZ   4.2
 -3.363 -3.645 -3.922 -4.192                                            TZ   4.3
  0.000   .006   .014   .026   .039   .053   .079   .131   .248   .315  TZ   5.1
   .290   .200  -.074  -.445  -.874 -1.341 -1.586 -1.832 -2.078 -2.326  TZ   5.2
 -2.574 -2.819 -3.059 -3.300                                            TZ   5.3
  0.000   .005   .011   .020   .031   .042   .063   .101   .198   .304  TZ   6.1
   .315   .272   .105  -.148  -.455  -.798  -.978 -1.161 -1.351 -1.541  TZ   6.2
 -1.732 -1.925 -2.118 -2.309                                            TZ   6.3
  0.000   .004   .007   .016   .026   .032   .046   .073   .119   .206  TZ   7.1
   .229   .206   .110  -.003  -.192  -.393  -.503  -.613  -.732  -.850  TZ   7.2
  -.969 -1.090 -1.212 -1.326                                            TZ   7.3
  0.000   .003   .005   .009   .013   .016   .023   .036   .069   .120  TZ   8.1
   .157   .165   .138   .069  -.027  -.145  -.212  -.282  -.356  -.433  TZ   8.2
  -.511  -.593  -.678  -.763                                            TZ   8.3
  0.000   .002   .003   .005   .009   .011   .017   .027   .050   .086  TZ   9.1
   .112   .120   .105   .054  -.022  -.121  -.176  -.234  -.296  -.361  TZ   9.2
  -.428  -.497  -.569  -.643                                            TZ   9.3

  0.000  0.000  0.000  0.000   .002   .005   .009   .018   .037   .066  TZ  10.1
   .086   .091   .076   .037  -.017  -.077  -.110  -.145  -.181  -.218  TZ  10.2
  -.256  -.294  -.336  -.375                                            TZ  10.3
  0.000  0.000  0.000  0.000   .002   .005   .009   .018   .037   .066  TZ  11.1
   .086   .091   .076   .037  -.017  -.077  -.110  -.145  -.181  -.218  TZ  11.2
  -.256  -.294  -.336  -.375                                            TZ  11.3
  0.000  0.000  0.000  0.000  0.000  0.000  0.000  0.000  0.000  0.000  TZ  12.1
  0.000  0.000  0.000  0.000  0.000  0.000  0.000  0.000  0.000  0.000  TZ  12.2
  0.000  0.000  0.000  0.000                                            TZ  12.3
0.00   .182   .253   .345   .405   .447   .500   .582   .742   .958    WORD 1.1
1.115  1.221  1.390  1.440  1.410  1.259  1.147  1.015   .866   .695    WORD 1.2
.525   .352   .179   0.                                                WORD 1.3
0.00   .182   .253   .345   .405   .447   .500   .582   .728   .925    WORD 2.1
1.040  1.175  1.325  1.374  1.340  1.201  1.094  .9685   .826   .663    WORD 2.2
.501   .336   .171   0.                                                WORD 2.3
0.00   .182   .253   .345   .405   .447   .500   .582   .708   .889    WORD2A.1
1.015  1.110  1.230  1.281  1.255  1.120  1.020   .904   .770   .623    WORD2A.2
.470   .315   .161   0.0                                               WORD2A.3
0.00   .182   .253   .345   .405   .447   .500   .582   .692   .837    WORD 3.1
.972  1.035  1.174  1.218  1.193  1.065   .970   .859   .733   .593    WORD 3.2
.447   .300   .153   0.                                                WORD 3.3
0.00   .182   .253   .345   .405   .447   .500   .582   .700   .865    WORD 4.1
.980  1.065  1.189  1.230  1.205  1.076   .98    .867   .740   .599    WORD 4.2
.452   .303   .154   0.                                                WORD 4.3
0.00   .182   .253   .345   .405   .447   .500   .582   .708   .880    WORD 5.1
1.00  1.090  1.218  1.263  1.237  1.104  1.006   .890   .760   .615    WORD 5.2
.464   .311   .159   0.                                                WORD 5.3
0.00   .182   .253   .345   .405   .447   .500   .582   .710   .885    WORD 6.1
1.005  1.100  1.229  1.276  1.250  1.116  1.016   .90    .767   .621    WORD 6.2
.468   .314   .160   0.                                                WORD 6.3
0.00   .198   .275   .371   .431   .470   .527   .600   .725   .885    WORD 7.1
1.010  1.110  1.240  1.293  1.266  1.131  1.030   .911   .778   .629    WORD 7.2
.475   .319   .162   0.                                                WORD 7.3
0.00   .198   .275   .371   .431   .470   .527   .600   .735   .912    WORD 8.1
1.048  1.152  1.283  1.338  1.310  1.170  1.066   .943   .805   .651    WORD 8.2
.491   .330   .168   0.                                                WORD 8.3
0.00   .198   .275   .371   .431   .470   .530   .618   .745   .928    WORD 9.1
1.059  1.160  1.304  1.356  1.328  1.186  1.080   .956   .816   .660    WORD 9.2
.498   .334   .170   0.                                                WORD 9.3
0.00   .198   .275   .371   .431   .470   .530   .600   .738   .928    WORD10.1
1.070  1.182  1.331  1.388  1.359  1.214  1.105   .978   .835   .675    WORD10.2
.510   .342   .174   0.                                                WORD10.3
0.00   .008   .017   .034   .051   .067   .102   .166   .325   .608    WORD11.1
.845  1.041  1.302  1.388  1.359  1.214  1.105   .978   .835   .675    WORD11.2
.510   .342   .174   0.                                                WORD11.3
0.0    .008   .017   .034   .051   .067   .102   .166   .322   .602    WORD12.1
.837  1.031  1.290  1.375  1.347  1.202  1.095   .969   .827   .669    WORD12.2
.505   .339   .173   0.                                                WORD12.3
0.0    9.144 18.288 27.432 32.004 36.576 41.148 45.720 50.292 54.864   XFUS 10
59.436 64.008 73.152 82.296 91.440 109.728128.016146.304164.59217A.308  XFUS 20
187.452196.596205.740                                                   XFUS 23
0.0    .128   .183   .192   .201   .201   .192   .174   .101  -.046    ZFUS 10
 -.347  -.686 -1.490 -2.377 -3.338 -5.157 -6.739 -8.120 -9.345 -10.222  ZFUS 20
-10.781-11.302-11.695                                                   ZFUS 23
0.0    8.823 25.669 43.646 55.686 67.392 77.443 85.703 91.974 94.817    FUSA 10
96.155 96.321 92.228 90.385 90.385 92.726 97.494 99.917 97.158 93.479   FUSA 20
89.298 82.609 74.499                                                    FUSA 23
```

TABLE II.- Concluded

(b) U.S. Customary Units. All dimensions are in inches

```
  1  1  1  1  1  1    13 24  4 25  7 22  9 28  9 27  8  2 10  2 10  1 10
1291.98                                                                    REFA
0.      .125    .25     .5      .75    1.0    1.5    2.5    5.0    10.      XAF 10
15.     20.     30.     40.     50.    60.    65.    70.    75.    80.      XAF 20
85.     90.     95.    100.                                                XAF
 22.282  2.012 -1.465 58.812                                               WORG1
 23.741  2.431 -1.847 57.380                                               WORG 2
 27.191  3.420 -2.444 53.910                                               WORG 2A
 32.219  4.862 -2.988 48.852                                               WORG 3
 40.696  7.293 -3.600 40.325                                               WORG4
 44.140  8.280 -3.823 36.860                                               WORG 5
 49.173  9.723 -4.129 32.217                                               WORG 6
 56.192 11.736 -4.417 25.742                                               WORG7
 61.573 13.608 -4.590 20.867                                               WORG 8
 64.381 14.585 -4.705 18.954                                               WORG9
 74.196 18.000 -5.069 12.265                                               WORG10
 74.196 18.000 -5.069 12.265                                               WORG11
85.968  24.800 -5.760  6.494                                               WORG 12
  0.000    .000    .000   0.000  -.000  -.001  -.003  -.009  -.047  -.187  TZ   1.1
  -.400   -.659  -1.246  -1.872 -2.498 -3.071 -3.319 -3.553 -3.773 -3.974  TZ   1.2
 -4.162  -4.331  -4.478  -4.608                                             TZ   1.3
  0.000    .000    .001    .001   .001   .001   .000  -.002  -.016  -.122  TZ   2.1
  -.295   -.515  -1.015  -1.577 -2.153 -2.664 -2.891 -3.114 -3.326 -3.539  TZ   2.2
 -3.726  -3.899  -4.043  -4.165                                             TZ   2.3
  0.000    .001    .002    .005   .007   .009   .013   .021   .032   .025  TZ  2A.1
  -.155   -.317   -.709  -1.148 -1.602 -2.038 -2.236 -2.437 -2.632 -2.815  TZ  2A.2
 -2.988  -3.146  -3.290  -3.416                                             TZ  2A.3
  0.000    .002    .004    .007   .011   .014   .020   .031   .051   .021  TZ   3.1
  -.062   -.172   -.446   -.761 -1.096 -1.436 -1.604 -1.769 -1.931 -2.087  TZ   3.2
 -2.238  -2.382  -2.519  -2.647                                             TZ   3.3
  0.000    .002    .004    .008   .012   .017   .025   .040   .075   .089  TZ   4.1
   .062    .012   -.134   -.319  -.528  -.752  -.866  -.981 -1.096 -1.211  TZ   4.2
 -1.324  -1.435  -1.544  -1.650                                             TZ   4.3
  0.000    .003    .005    .010   .015   .021   .031   .051   .098   .124  TZ   5.1
   .114    .079   -.029   -.175  -.344  -.528  -.624  -.721  -.818  -.916  TZ   5.2
 -1.013  -1.110  -1.204  -1.299                                             TZ   5.3
  0.000    .002    .004    .008   .012   .017   .025   .040   .078   .120  TZ   6.1
   .124    .107    .041   -.058  -.179  -.314  -.385  -.457  -.532  -.607  TZ   6.2
  -.682   -.758   -.834   -.909                                             TZ   6.3
  0.000    .001    .003    .006   .010   .013   .018   .029   .047   .081  TZ   7.1
   .090    .081    .043   -.001  -.076  -.155  -.198  -.241  -.288  -.335  TZ   7.2
  -.382   -.429   -.477   -.522                                             TZ   7.3
  0.000    .001    .002    .004   .005   .006   .009   .014   .027   .047  TZ   8.1
   .062    .065    .054    .027  -.010  -.057  -.084  -.111  -.140  -.170  TZ   8.2
  -.201   -.234   -.267   -.300                                             TZ   8.3
  0.000    .001    .001    .002   .004   .005   .007   .011   .020   .034  TZ   9.1
   .044    .047    .041    .021  -.009  -.048  -.069  -.092  -.117  -.142  TZ   9.2
  -.168   -.196   -.224   -.253                                             TZ   9.3
  0.000   0.000   0.000   0.000   .001   .002   .004   .007   .014   .026  TZ  10.1
   .034    .036    .030    .014  -.007  -.030  -.043  -.057  -.071  -.086  TZ  10.2
  -.101   -.116   -.132   -.148                                             TZ  10.3
  0.000   0.000   0.000   0.000   .001   .002   .004   .007   .014   .026  TZ  11.1
   .034    .036    .030    .014  -.007  -.030  -.043  -.057  -.071  -.086  TZ  11.2
  -.101   -.116   -.132   -.148                                             TZ  11.3
  0.000   0.000   0.000   0.000  0.000  0.000  0.000  0.000  0.000  0.000  TZ  12.1
  0.000   0.000   0.000   0.000  0.000  0.000  0.000  0.000  0.000  0.000  TZ  12.2
  0.000   0.000   0.000   0.000                                             TZ  12.3
0.00    .182    .253    .345    .405    .447    .500    .582    .742    .958  WORD 1.1
1.115   1.221   1.390   1.440   1.410   1.259   1.147   1.015    .866    .695  WORD 1.2
.525    .352    .179    0.                                                 WORD 1.3
0.00    .182    .253    .345    .405    .447    .500    .582    .728    .925  WORD 2.1
1.040   1.175   1.325   1.374   1.340   1.201   1.094   .9685    .826    .663  WORD 2.2
.501    .336    .171    0.                                                 WORD 2.3
0.00    .182    .253    .345    .405    .447    .500    .582    .708    .889  WORD2A.1
1.015   1.110   1.230   1.281   1.255   1.120   1.020    .904    .770    .623  WORD2A.2
.470    .315    .161    0.0                                                WORD2A.3
0.00    .182    .253    .345    .405    .447    .500    .582    .692    .837  WORD 3.1
.972   1.035   1.174   1.218   1.193   1.065    .970    .859    .733    .593  WORD 3.2
.447    .300    .153    0.                                                 WORD 3.3
0.00    .182    .253    .345    .405    .447    .500    .582    .700    .865  WORD 4.1
.980   1.065   1.189   1.230   1.205   1.076    .98     .867    .740    .599  WORD 4.2
.452    .303    .154    0.                                                 WORD 4.3
0.00    .182    .253    .345    .405    .447    .500    .582    .708    .880  WORD 5.1
1.00   1.090   1.218   1.263   1.237   1.104   1.006    .890    .760    .615  WORD 5.2
.464    .311    .159    0.                                                 WORD 5.3
0.00    .182    .253    .345    .405    .447    .500    .582    .710    .885  WORD 6.1
1.005   1.100   1.229   1.276   1.250   1.116   1.016    .90     .767    .621  WORD 6.2
.468    .314    .160    0.                                                 WORD 6.3
0.00    .198    .275    .371    .431    .470    .527    .600    .725    .885  WORD 7.1
1.010   1.110   1.240   1.293   1.266   1.131   1.030    .911    .778    .629  WORD 7.2
.475    .319    .162    0.                                                 WORD 7.3
0.00    .198    .275    .371    .431    .470    .527    .600    .735    .912  WORD 8.1
1.048   1.152   1.283   1.338   1.310   1.170   1.066    .943    .805    .651  WORD 8.2
.491    .330    .168    0.                                                 WORD 8.3
0.00    .198    .275    .371    .431    .470    .530    .618    .745    .928  WORD 9.1
1.059   1.160   1.304   1.356   1.328   1.186   1.080    .956    .816    .660  WORD 9.2
.498    .334    .170    0.                                                 WORD 9.3
0.00    .198    .275    .371    .431    .470    .530    .600    .738    .928  WORD10.1
1.070   1.182   1.331   1.388   1.359   1.214   1.105    .978    .835    .675  WORD10.2
.510    .342    .174    0.                                                 WORD10.3
0.00    .008    .017    .034    .051    .067    .102    .166    .325    .608  WORD11.1
.845   1.041   1.302   1.388   1.359   1.214   1.105    .978    .835    .675  WORD11.2
.510    .342    .174    0.                                                 WORD11.3
0.0     .008    .017    .034    .051    .067    .102    .166    .322    .602  WORD12.1
.837   1.031   1.290   1.375   1.347   1.202   1.095    .969    .827    .669  WORD12.2
.505    .339    .173    0.                                                 WORD12.3
0.0     3.6     7.2    10.8    12.6    14.4    16.2    18.0    19.8    21.6  XFUS 10
23.4    25.2    28.8    32.4    36.0    43.2    50.4    57.6    64.8    70.2  XFUS 20
73.8    77.4    81.0                                                       XFUS 23
0.0     .050    .072    .075    .079    .079    .075    .068    .039   -.018  ZFUS 10
-.137   -.270   -.587   -.936  -1.314 -2.030 -2.653 -3.197 -3.679 -4.025  ZFUS 20
-4.244  -4.449  -4.604                                                     ZFUS 23
0.0    1.374   3.978   6.765   8.631  10.446  12.066  13.284  14.256  14.696  FUSA 10
14.904  14.930  14.450  14.010  14.010  14.373  15.189  15.487  15.060  14.489  FUSA 20
13.841  12.804  11.547                                                     FUSA 23
```

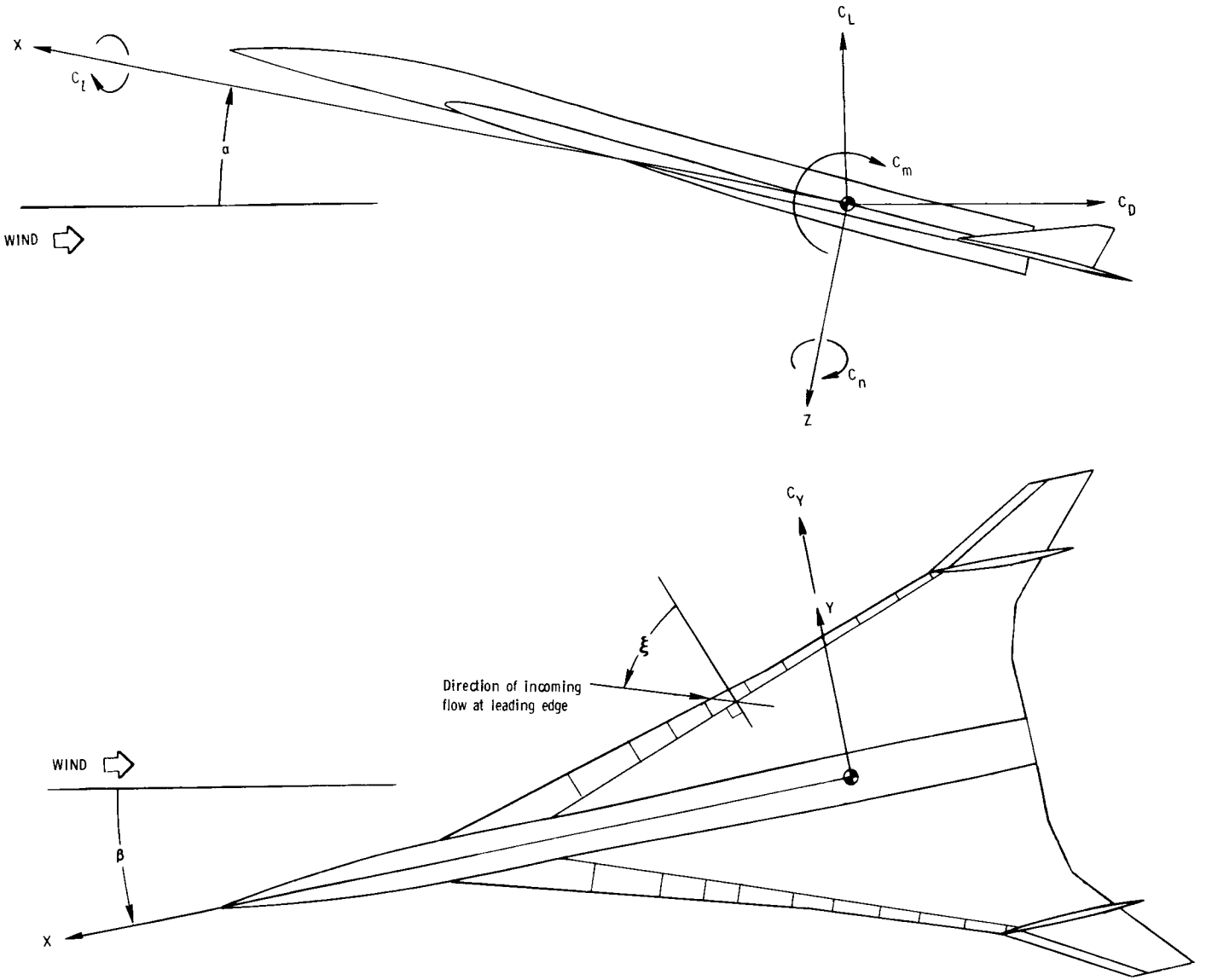

Figure 1.- System of axes and angular notation.

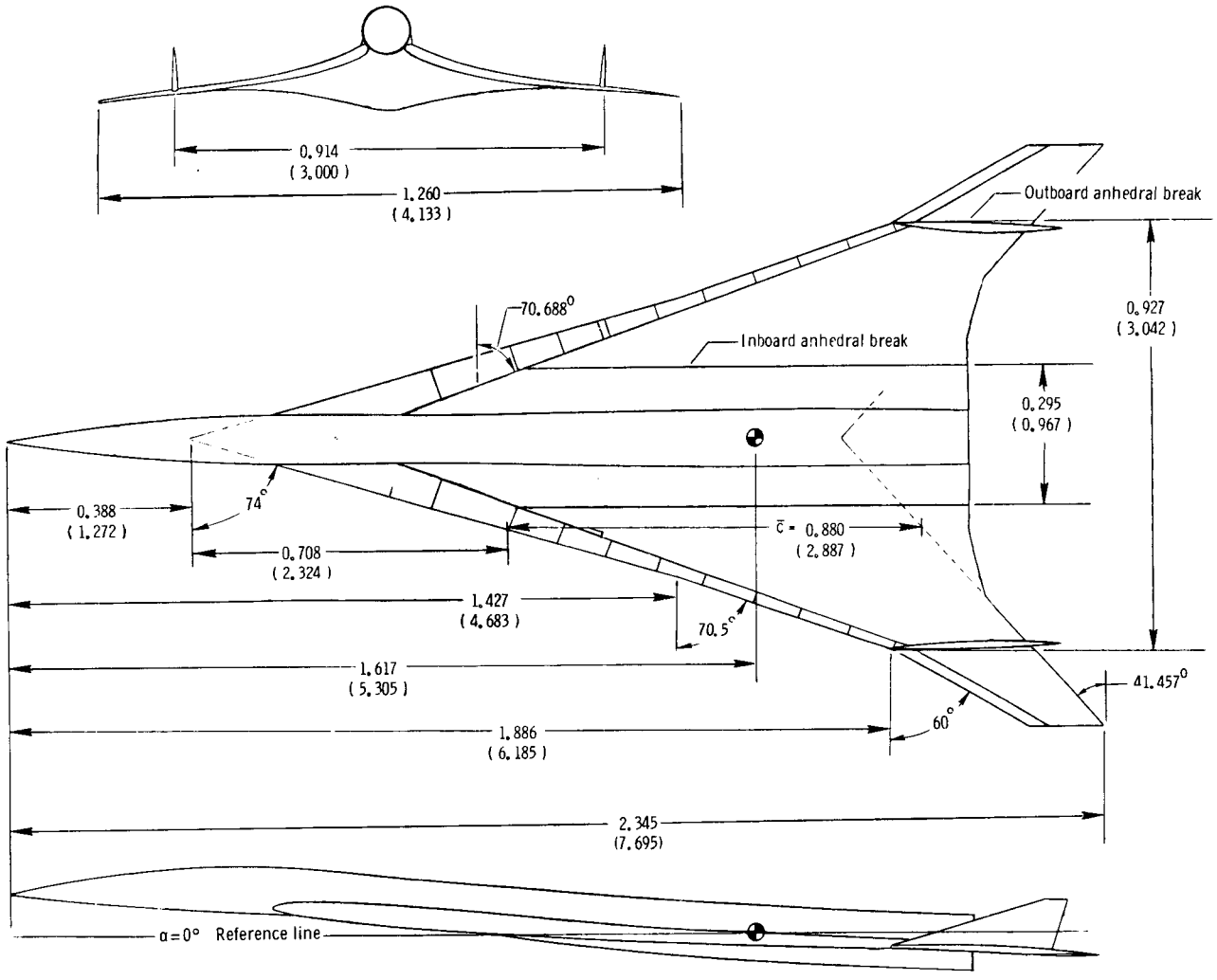

(a) Three-view sketch of model.

Figure 2.- Geometric characteristics. Dimensions are in meters (feet).

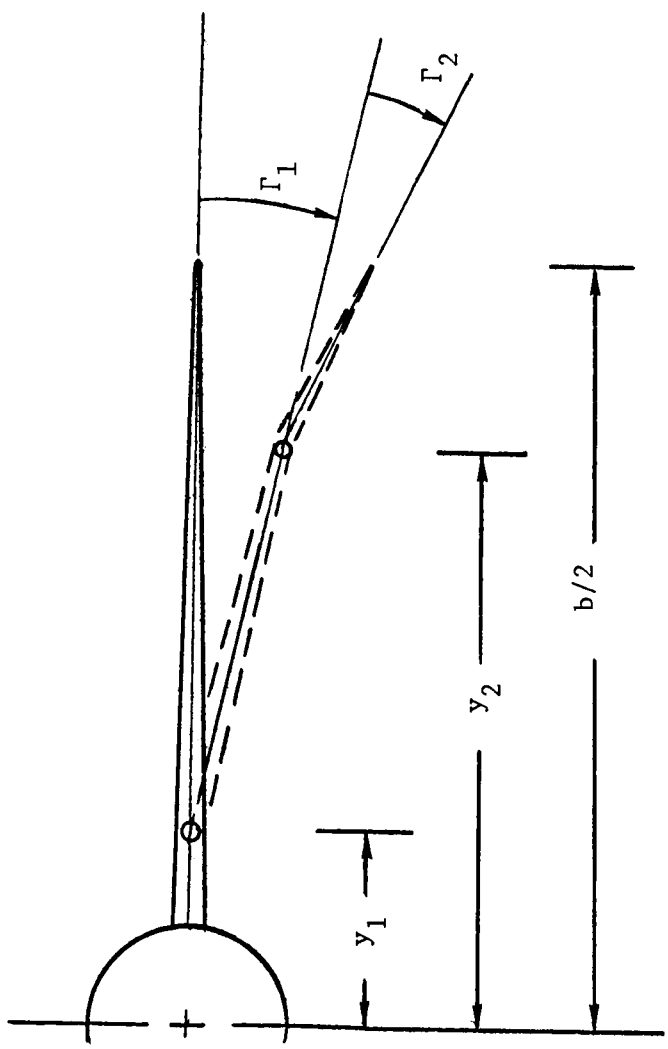

(b) Sketch showing anhedral angles.

Figure 2.- Concluded.

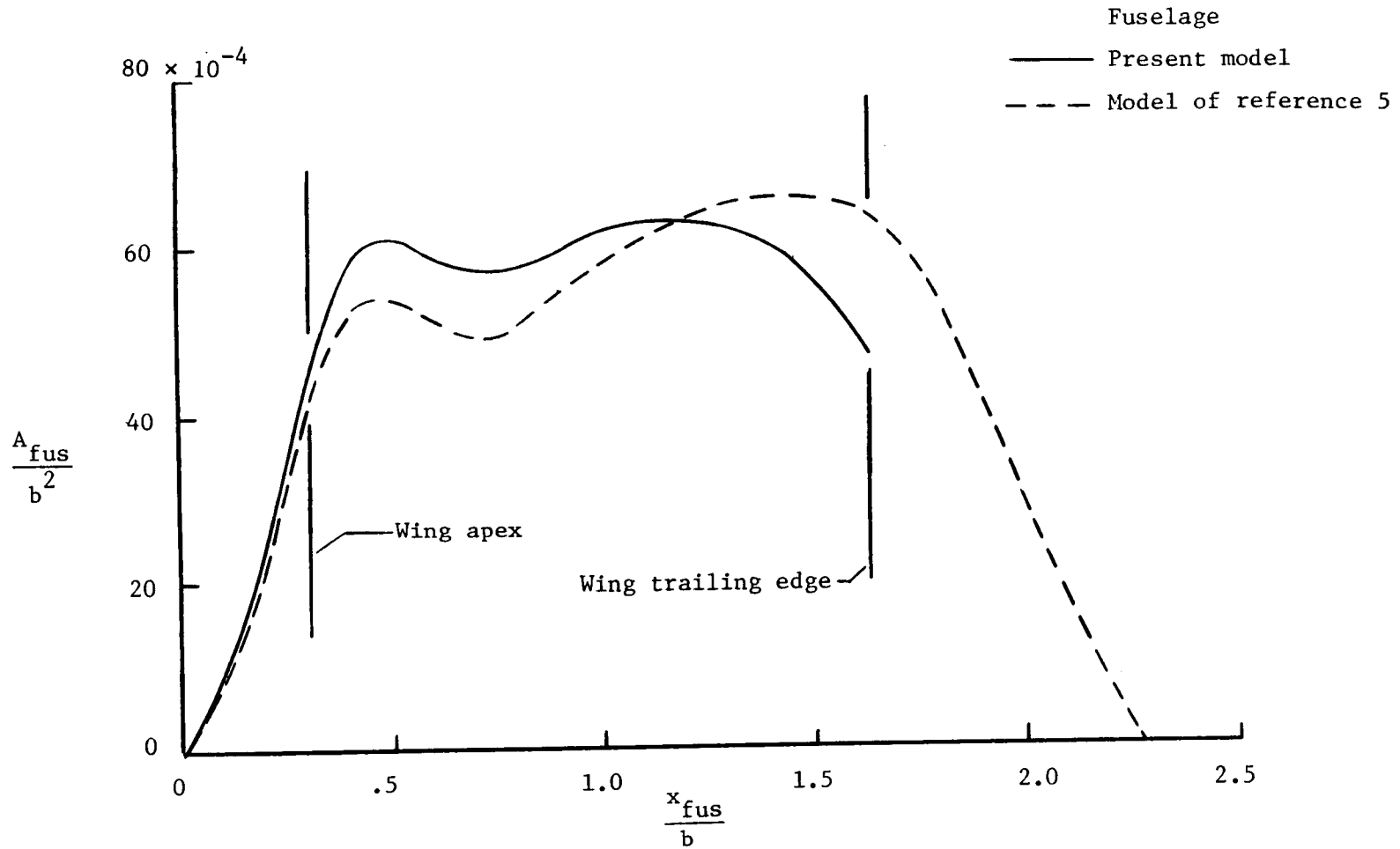

Figure 3.- Comparison of fuselage cross-sectional area distribution of present model and model of reference 5.

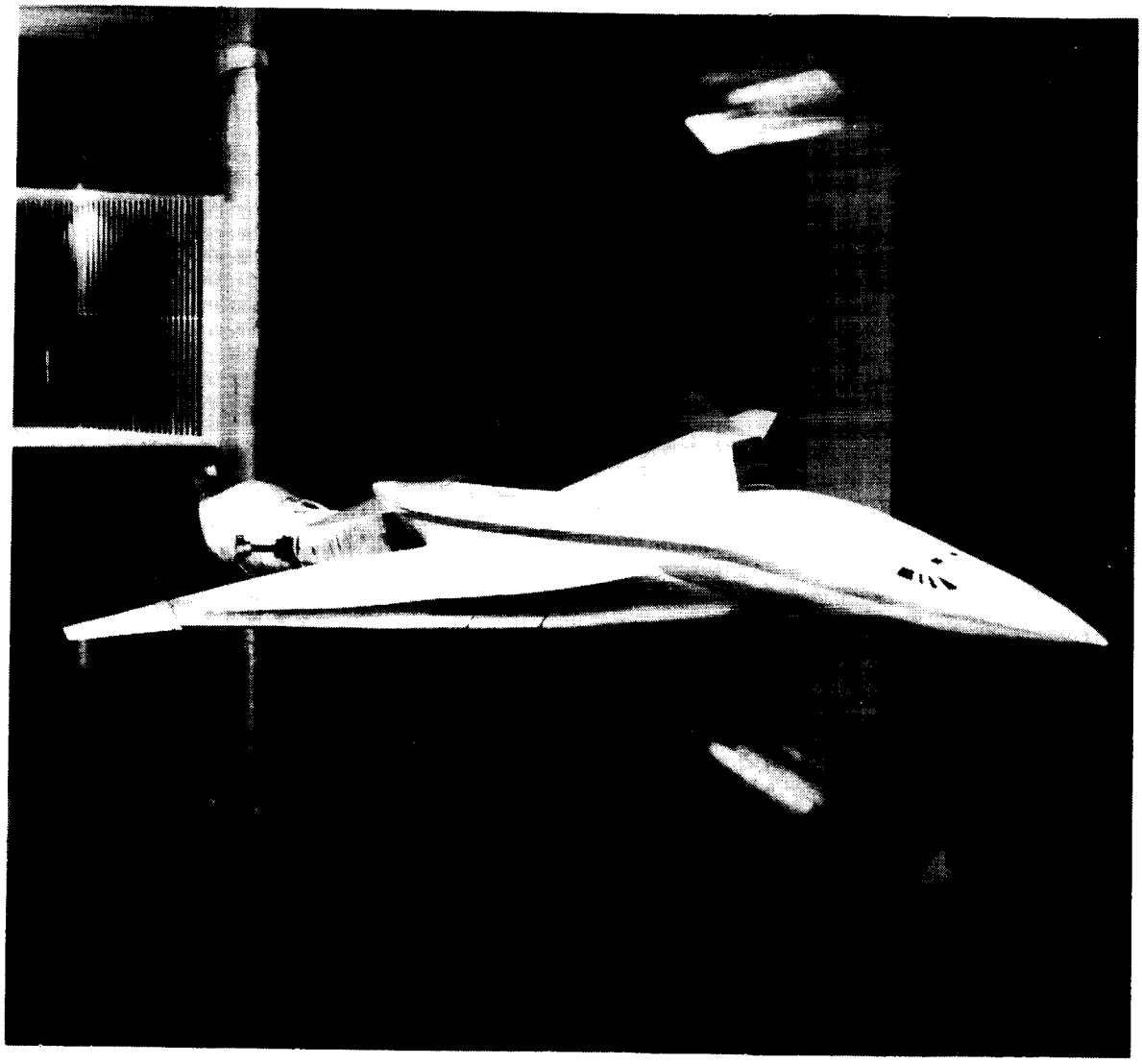

L-78-8188

Figure 4.- Photograph of model in Langley High-Speed 7- by 10-Foot Tunnel.

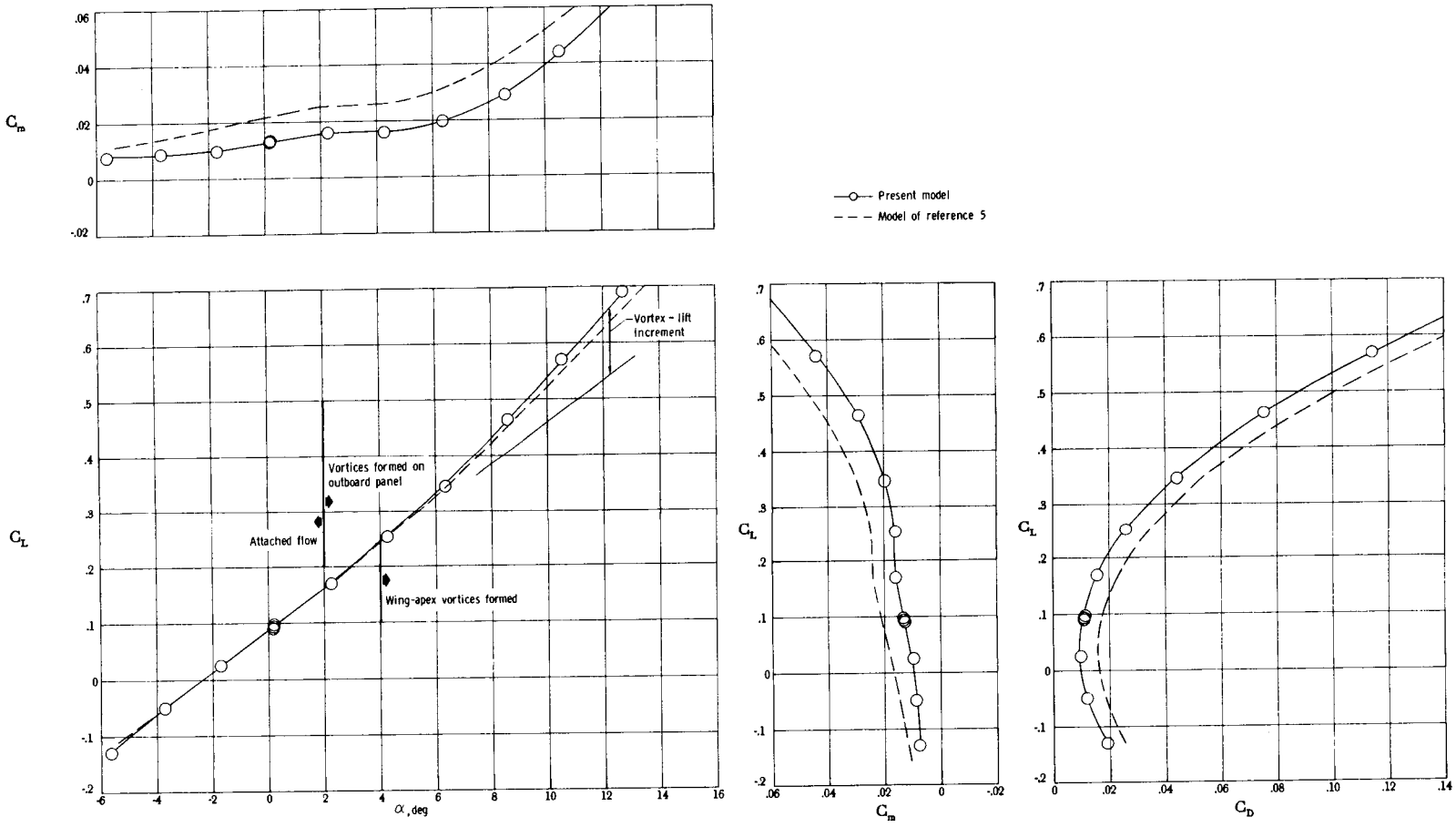

Figure 5.- Comparison of longitudinal aerodynamic data from present tests with data determined for related configuration of reference 5. $\delta_{L.E.} = 0^{o}$.

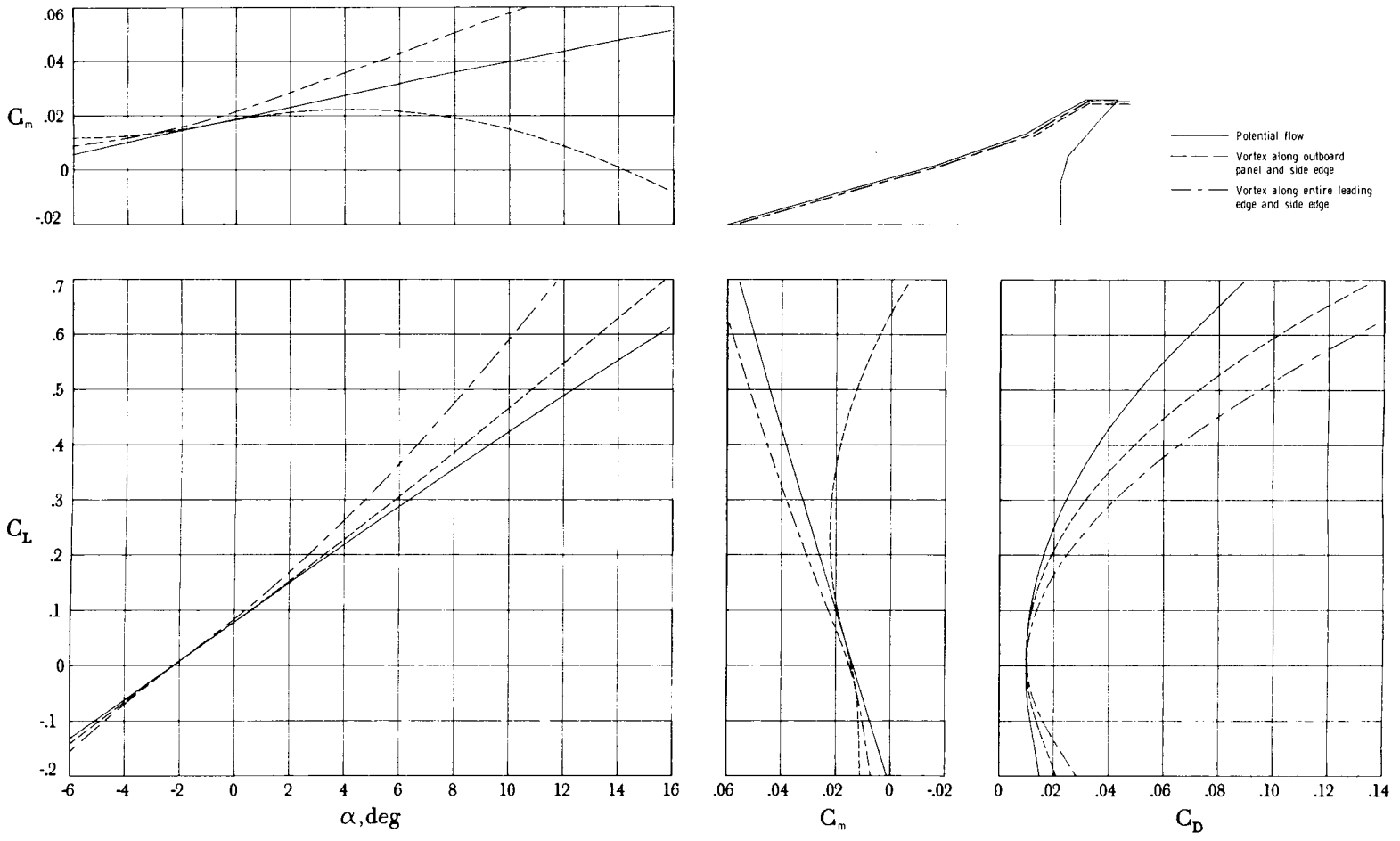

Figure 6.- Longitudinal aerodynamic characteristics predicted for twisted and cambered wing using the vortex-lattice method described in reference 12.

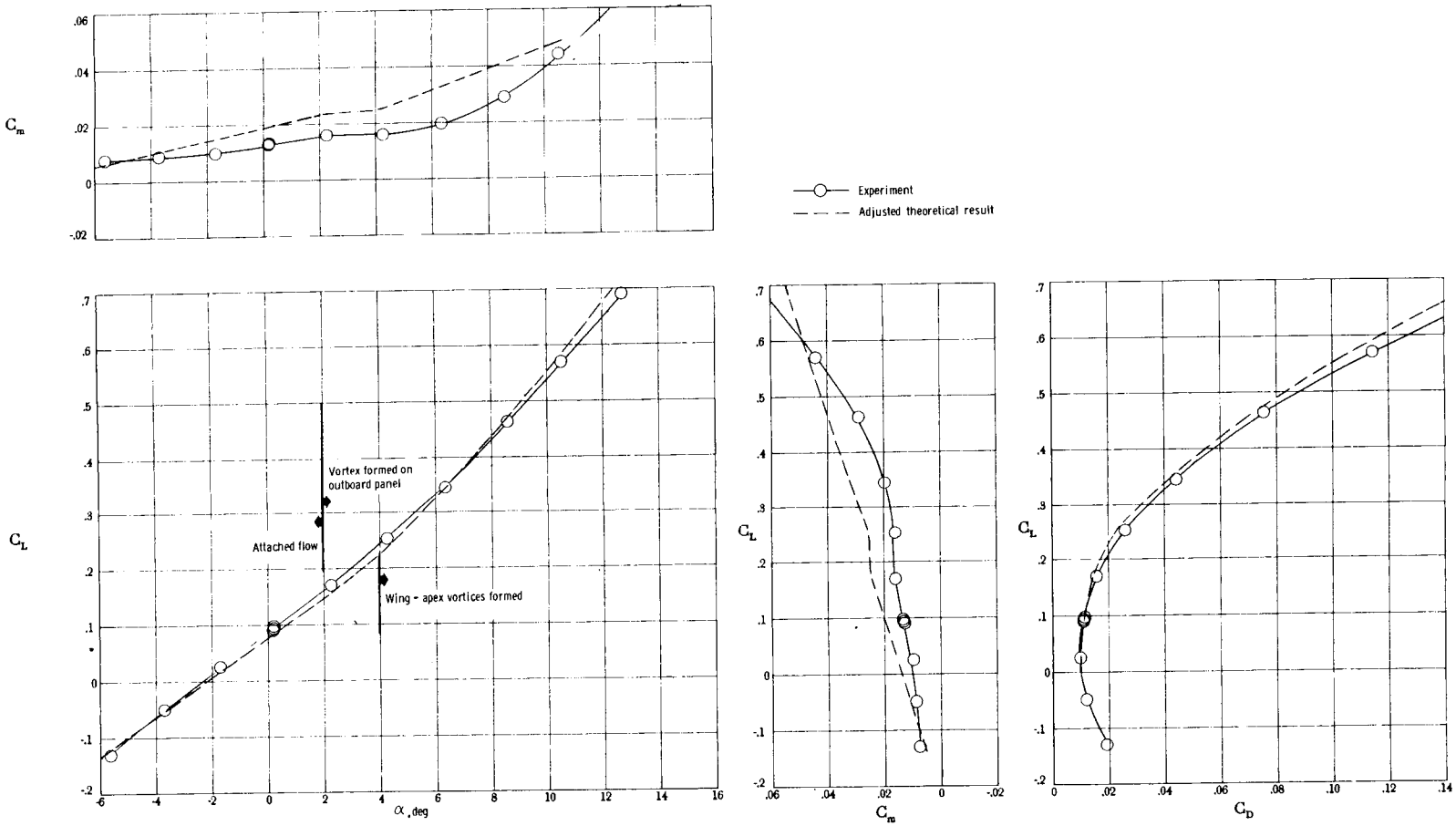

Figure 7.- Longitudinal aerodynamic characteristics of the configuration with $\delta_{L.E.} = 0^{o}$.

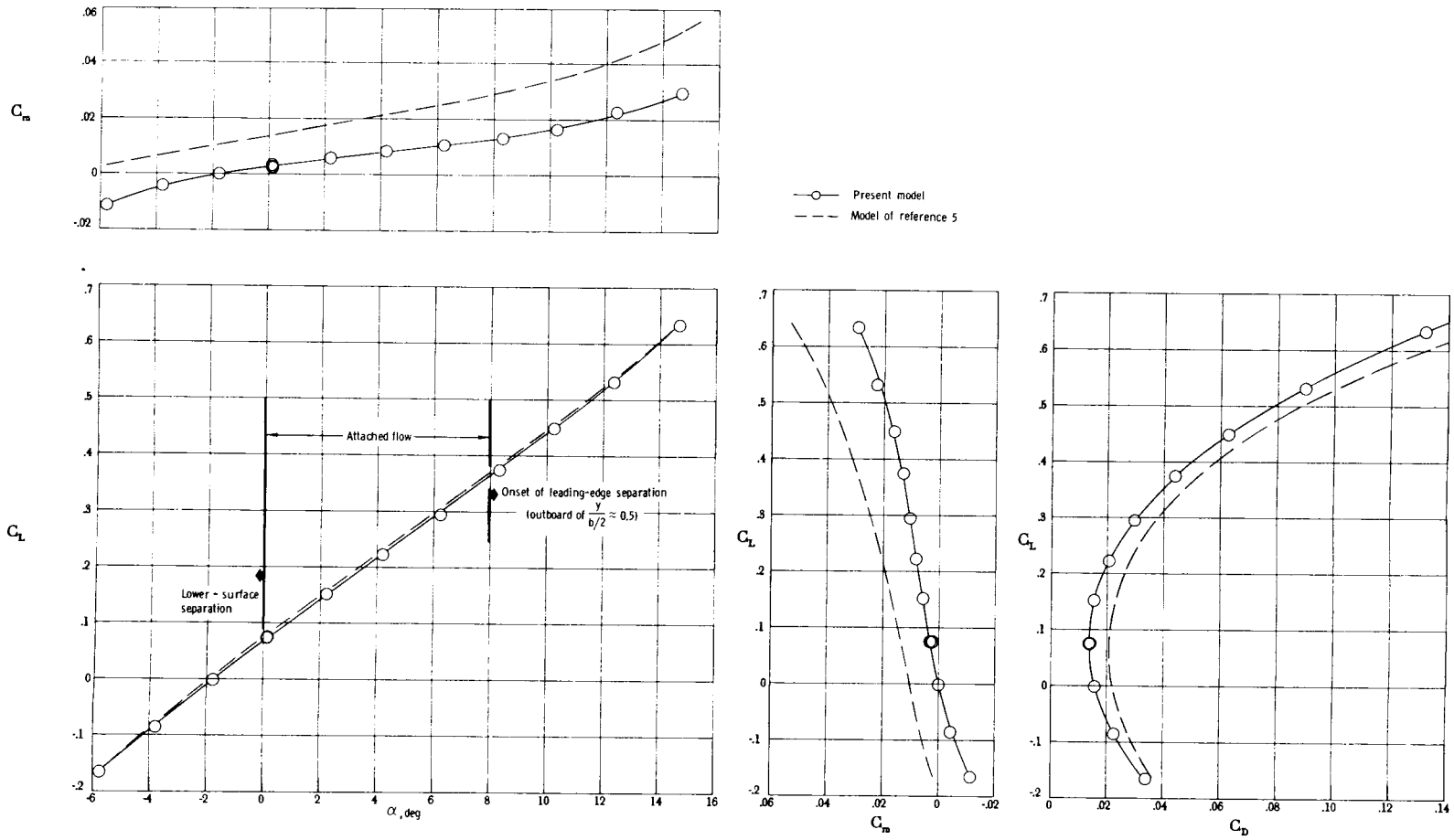

Figure 8.- Comparison of longitudinal aerodynamic data from present tests with data determined for related configuration of reference 5. $\delta_{L.E.} = 30^{o}$.

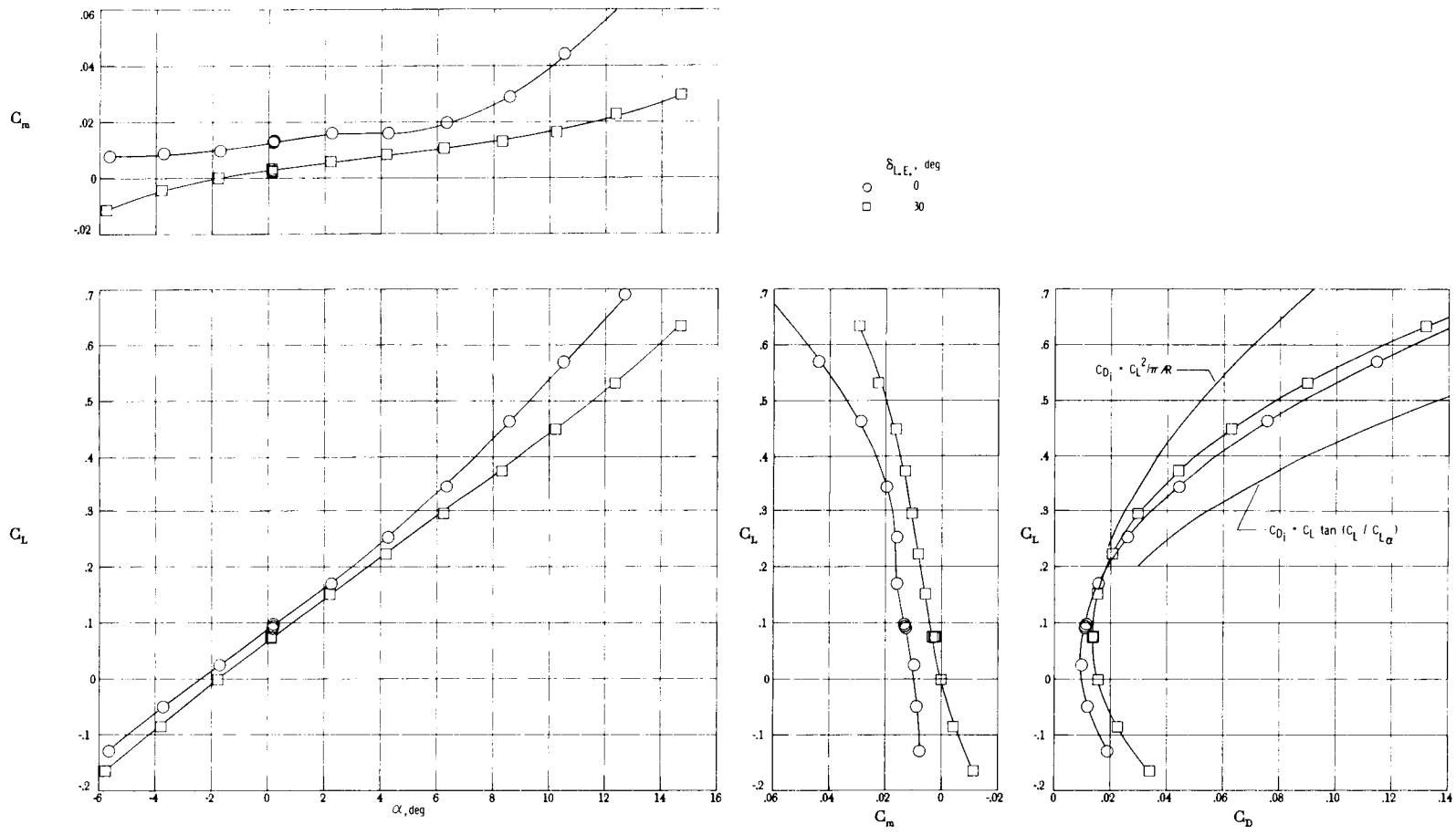

Figure 9.- Effect of wing leading-edge deflection on longitudianl aerodynamic characteristics.

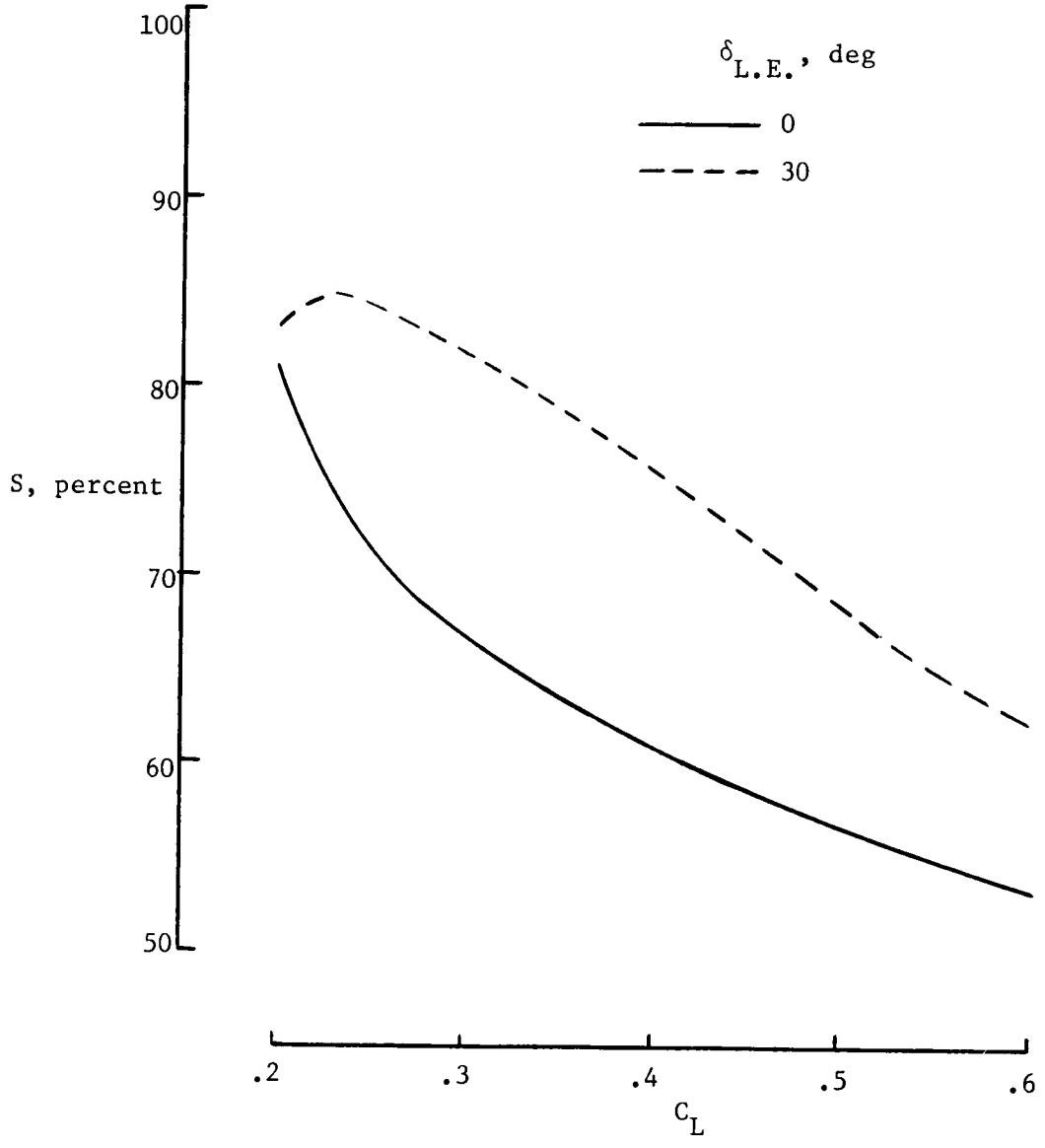

Figure 10.- Effect of leading-edge deflection on leading-edge suction.

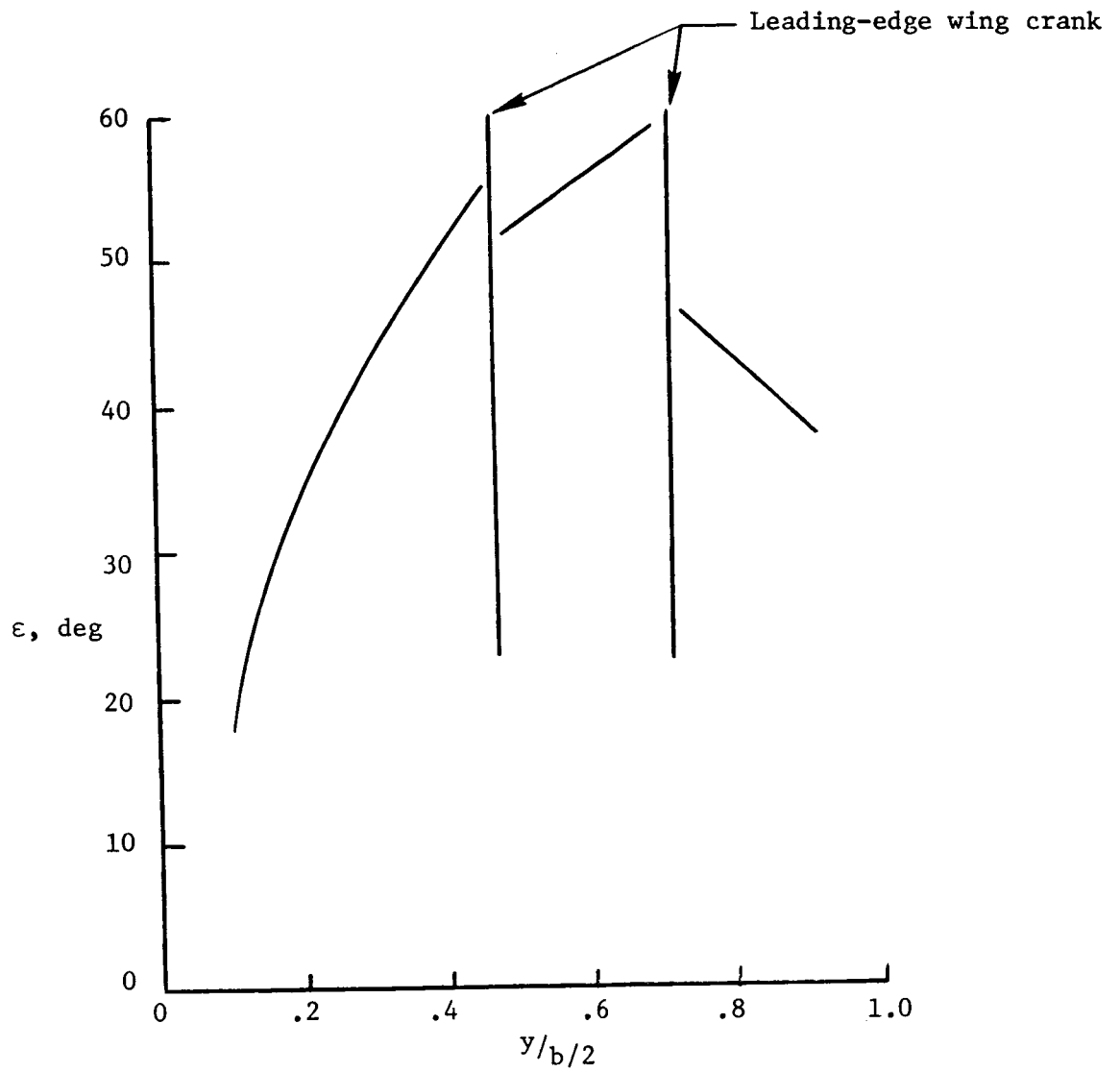

Figure 11.- Variation of theoretical upwash with nondimensional semispan. Theory based on vortex-lattice computational model. $\alpha = 10^{o}$ (ref. 5).

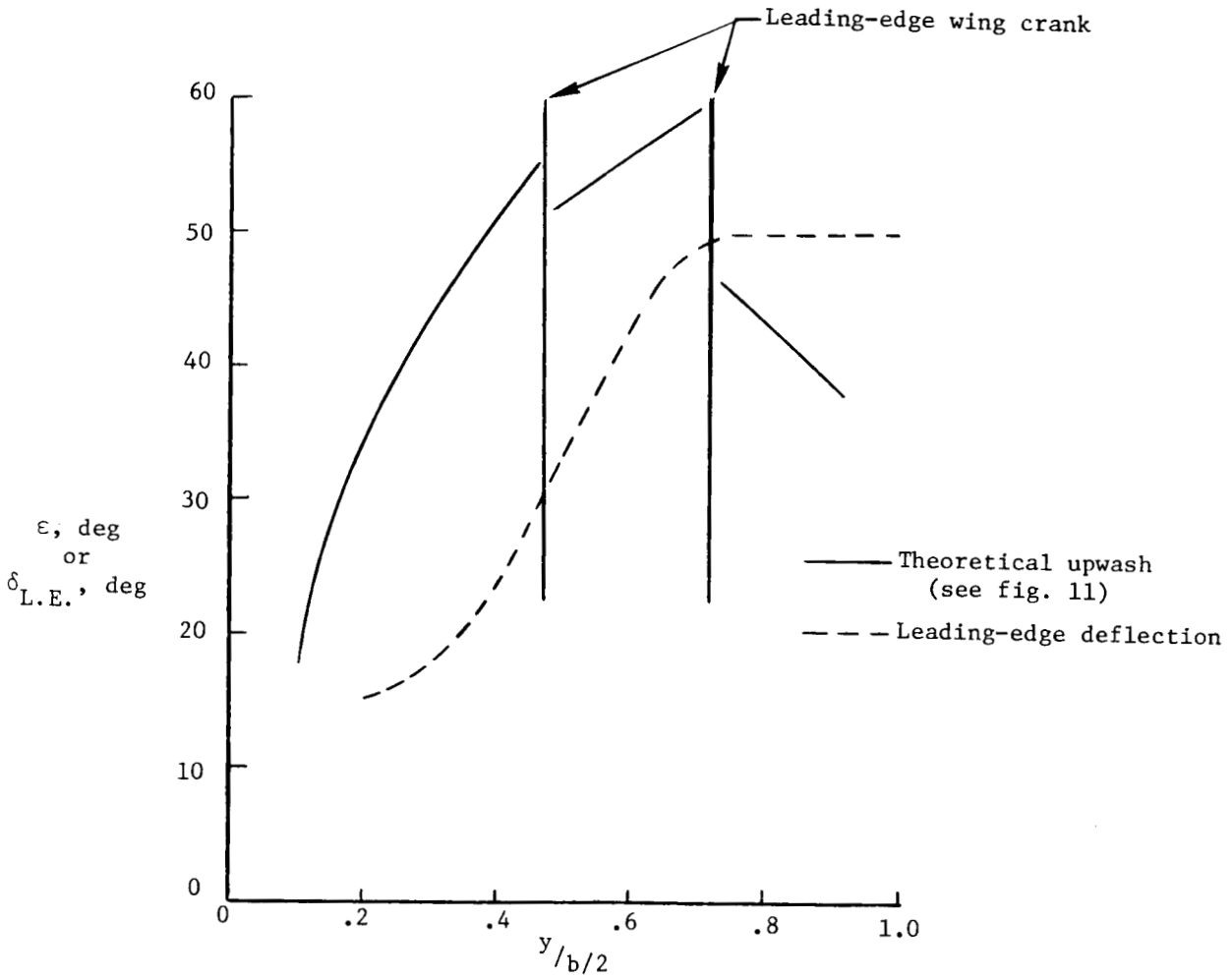

Figure 12.- Comparison of theoretical upwash with optimized leading-edge deflection.

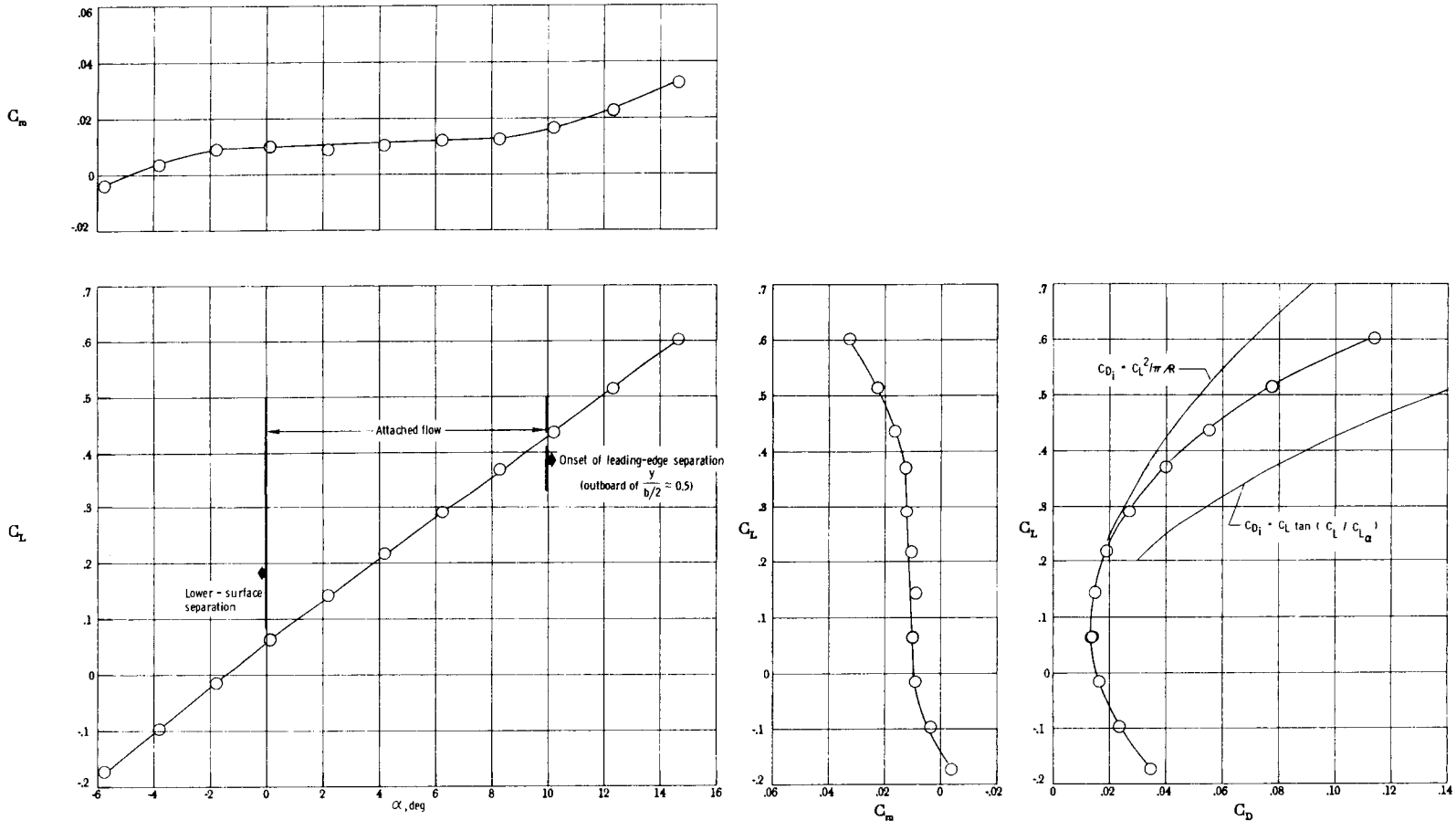

Figure 13.- Longitudinal aerodynamic characteristics for configuration with $\delta_{L.E.} = 16^o\text{-}50^o$.

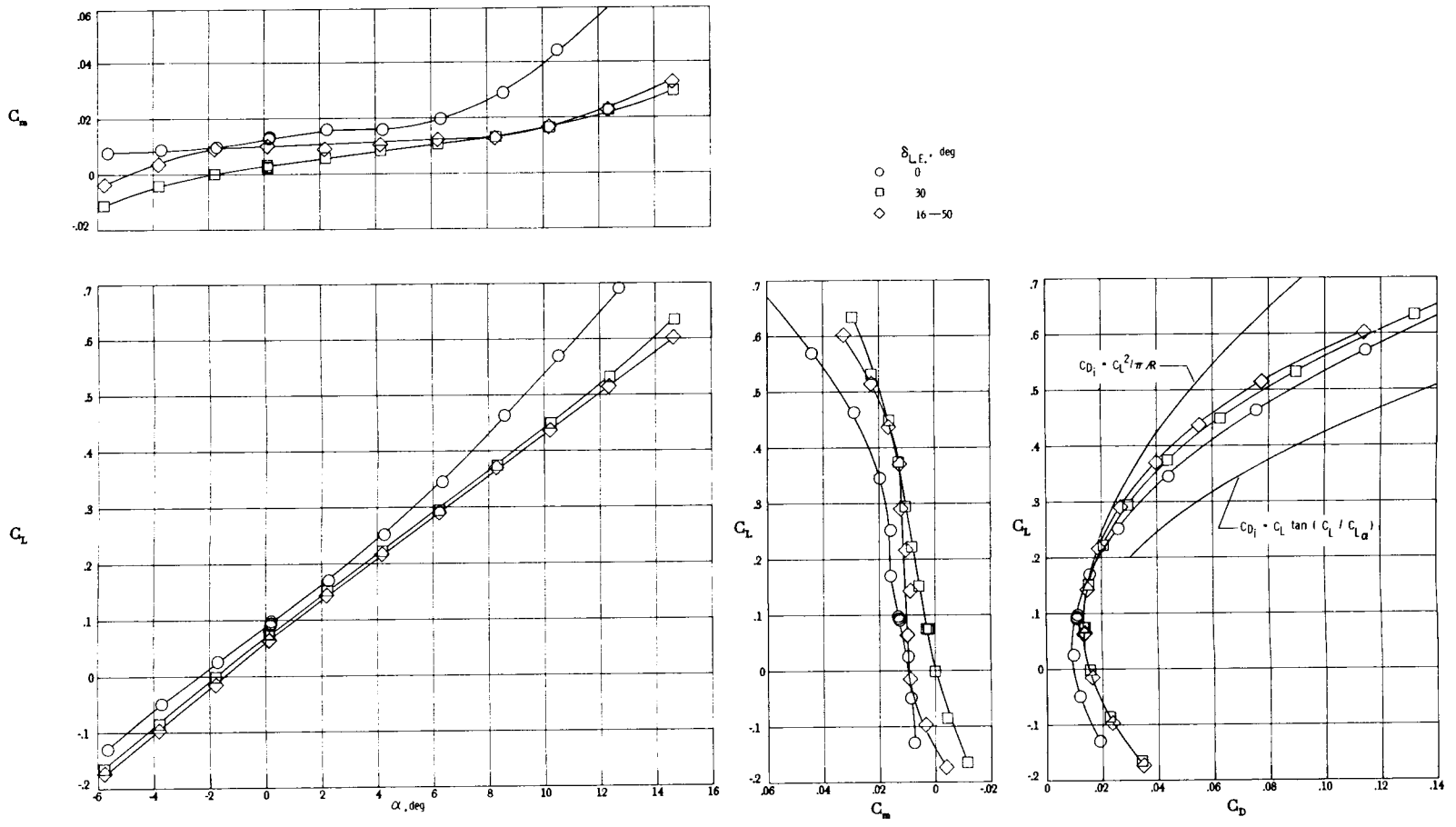

Figure 14.- Effect of wing leading-edge deflection on longitudinal aerodynamic characteristics.

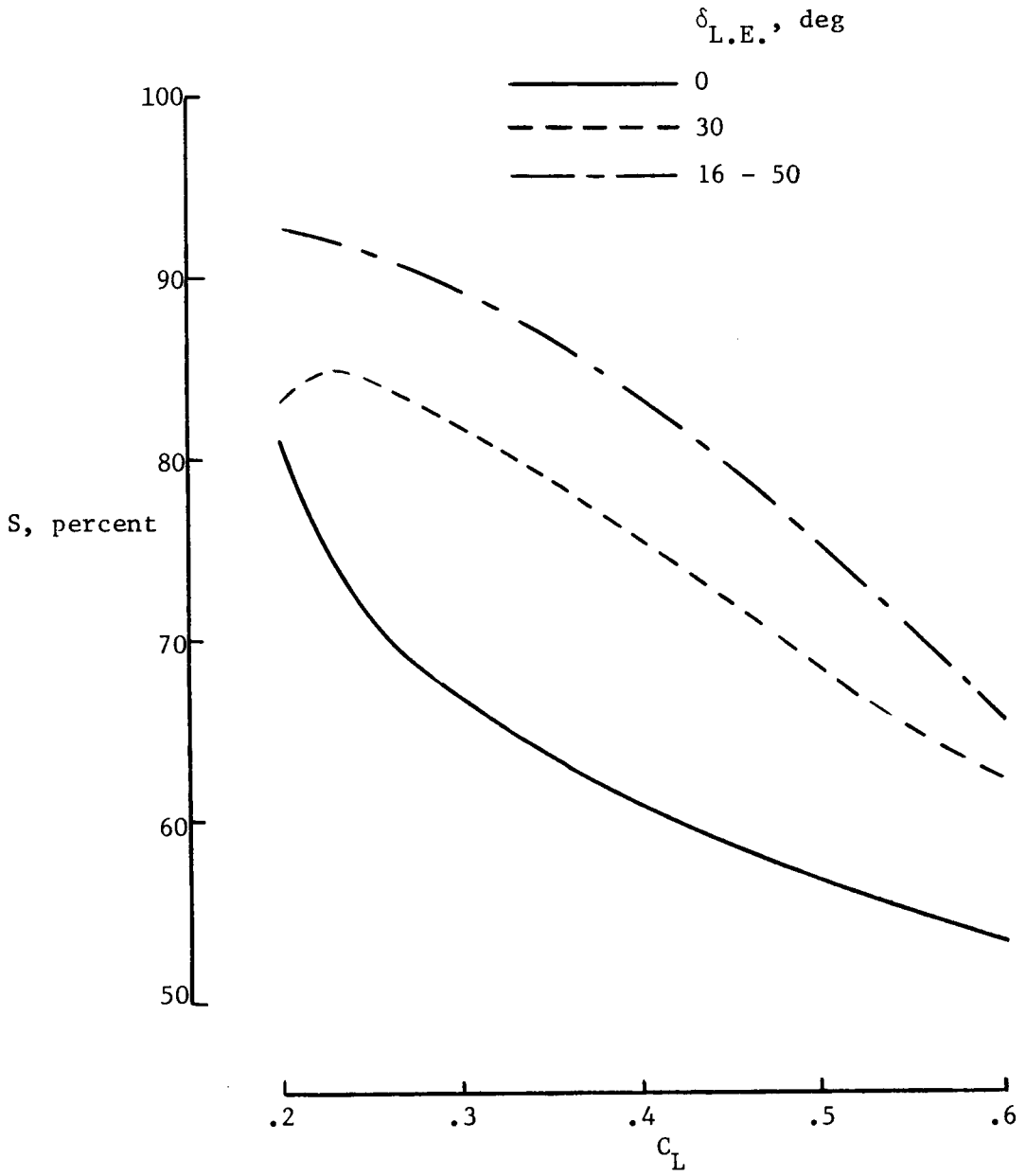

Figure 15.- Effect of continuously warped leading-edge deflection on leading-edge suction.

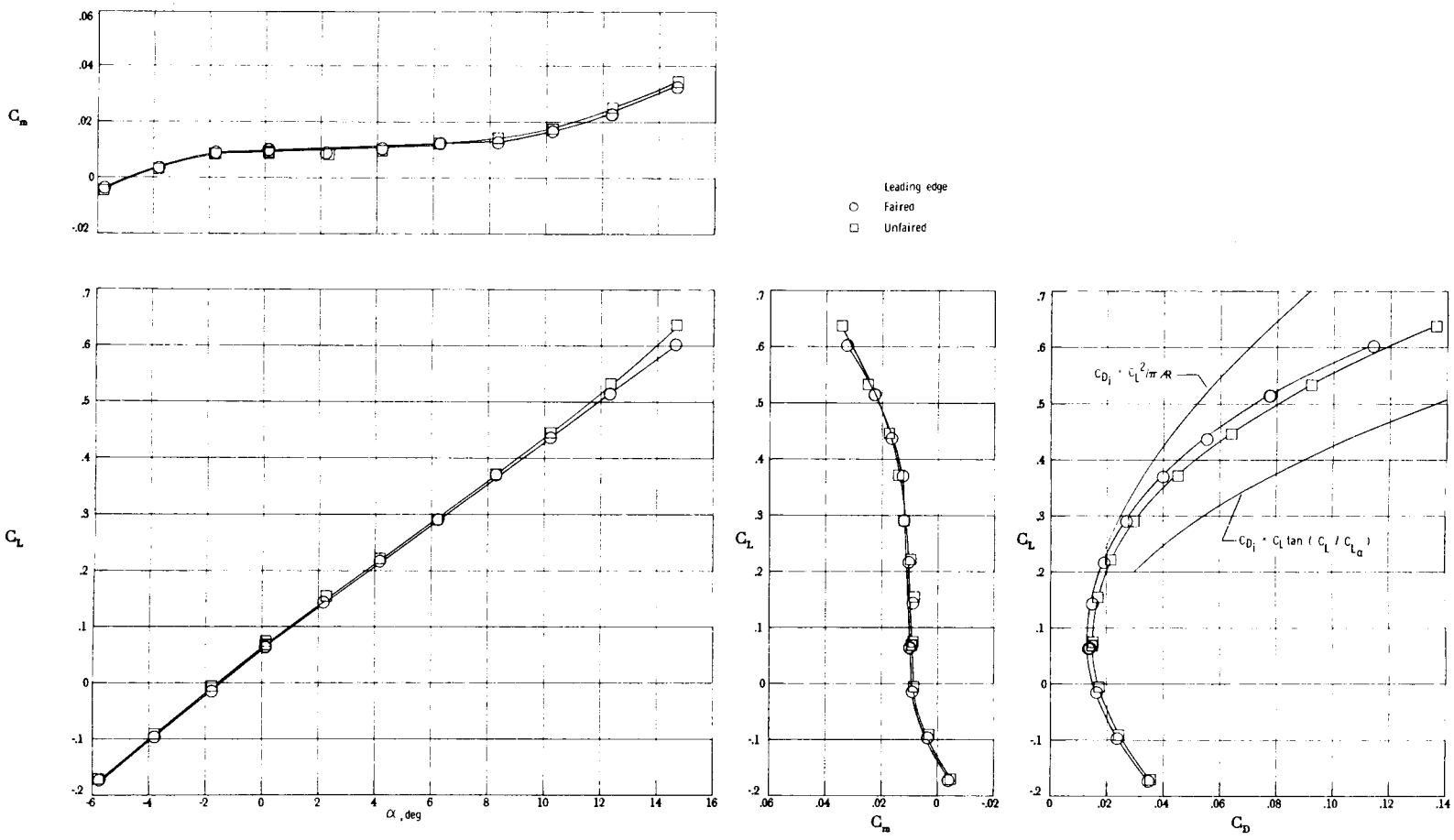

Figure 16.- Effect of removing fairings between adjacent segments of continuously warped leading edge. $\delta_{L.E.} = 16^{o}$-50^{o}.

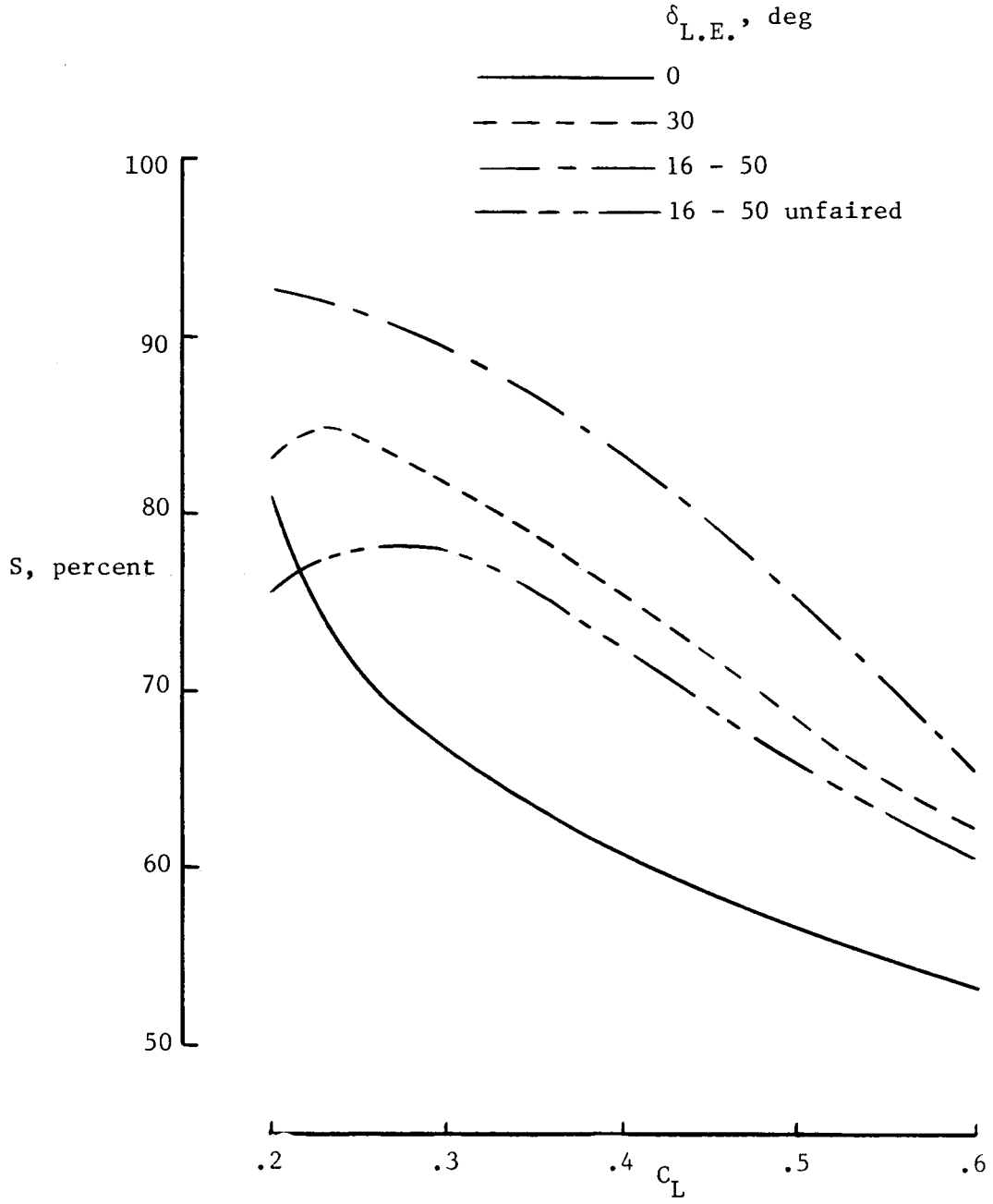

Figure 17.- Effect of removing fairings from adjacent segments of continuously warped leading edge.

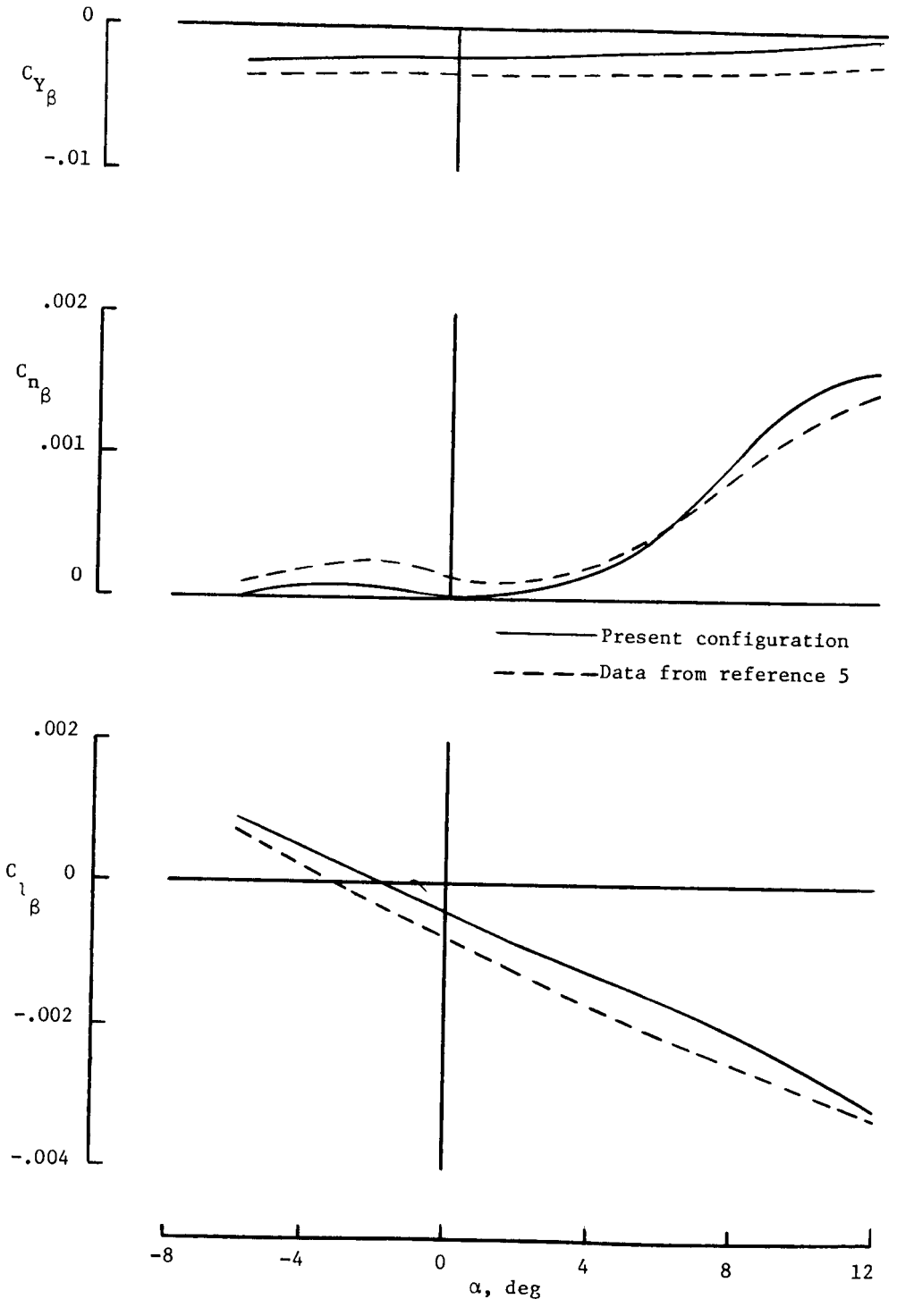

Figure 18.- Variation of lateral-directional stability derivatives with angle of attack. $\delta_{L.E.} = 0^{o}$.

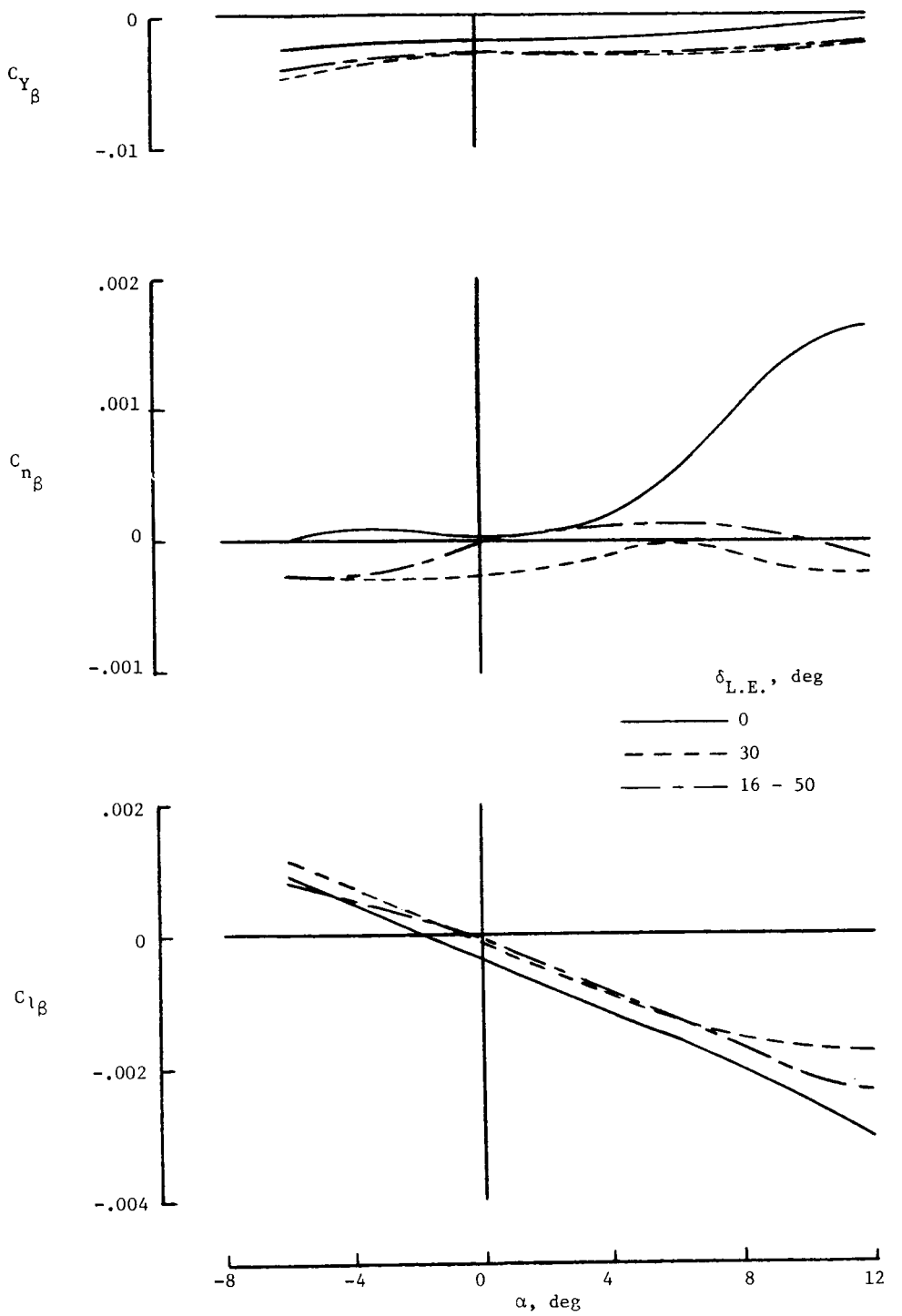

Figure 19.- Effect of leading-edge deflection on lateral-directional stability derivatives.

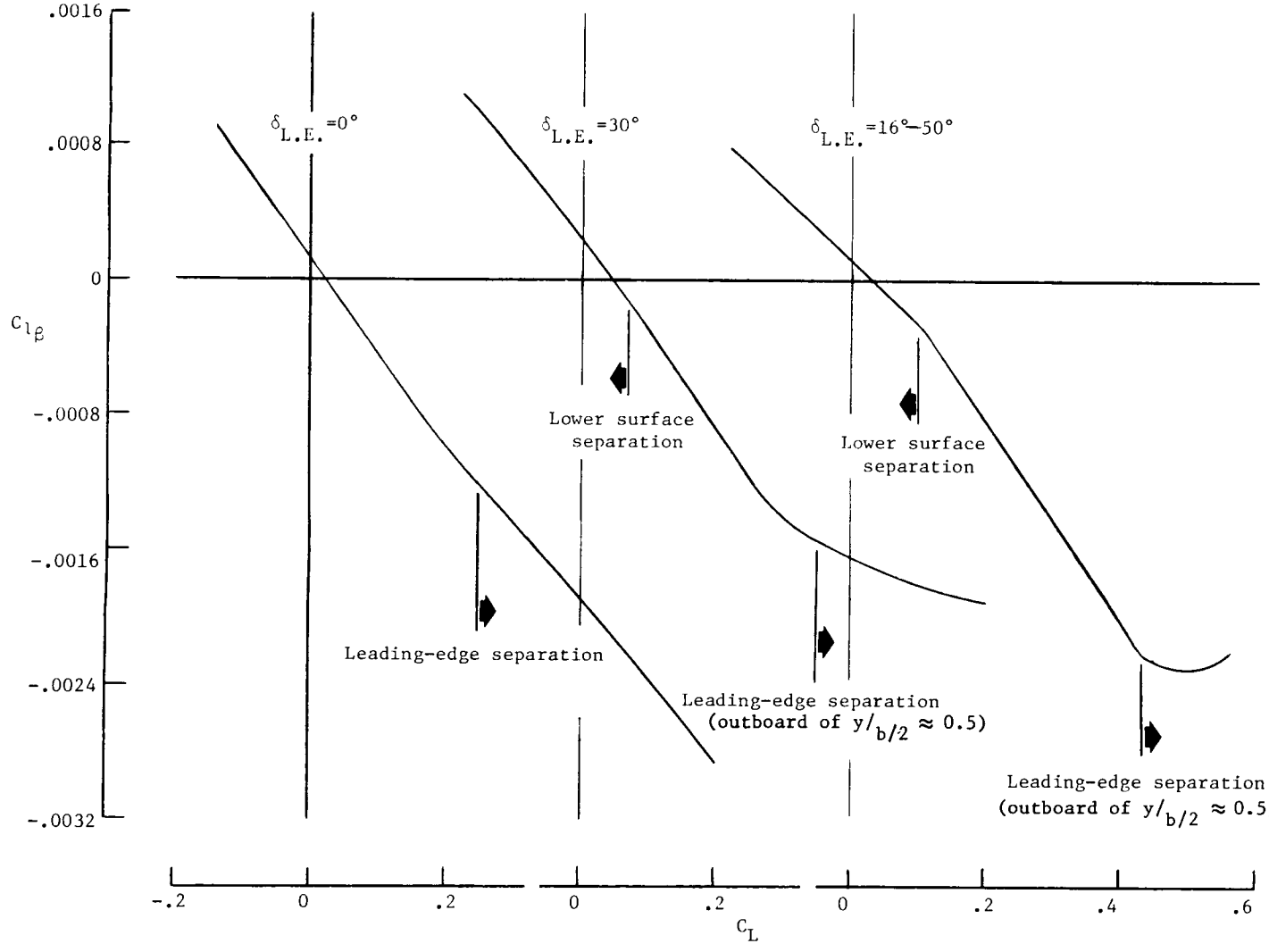

Figure 20.- Effect of leading-edge deflection on C_{l_β} versus C_L.

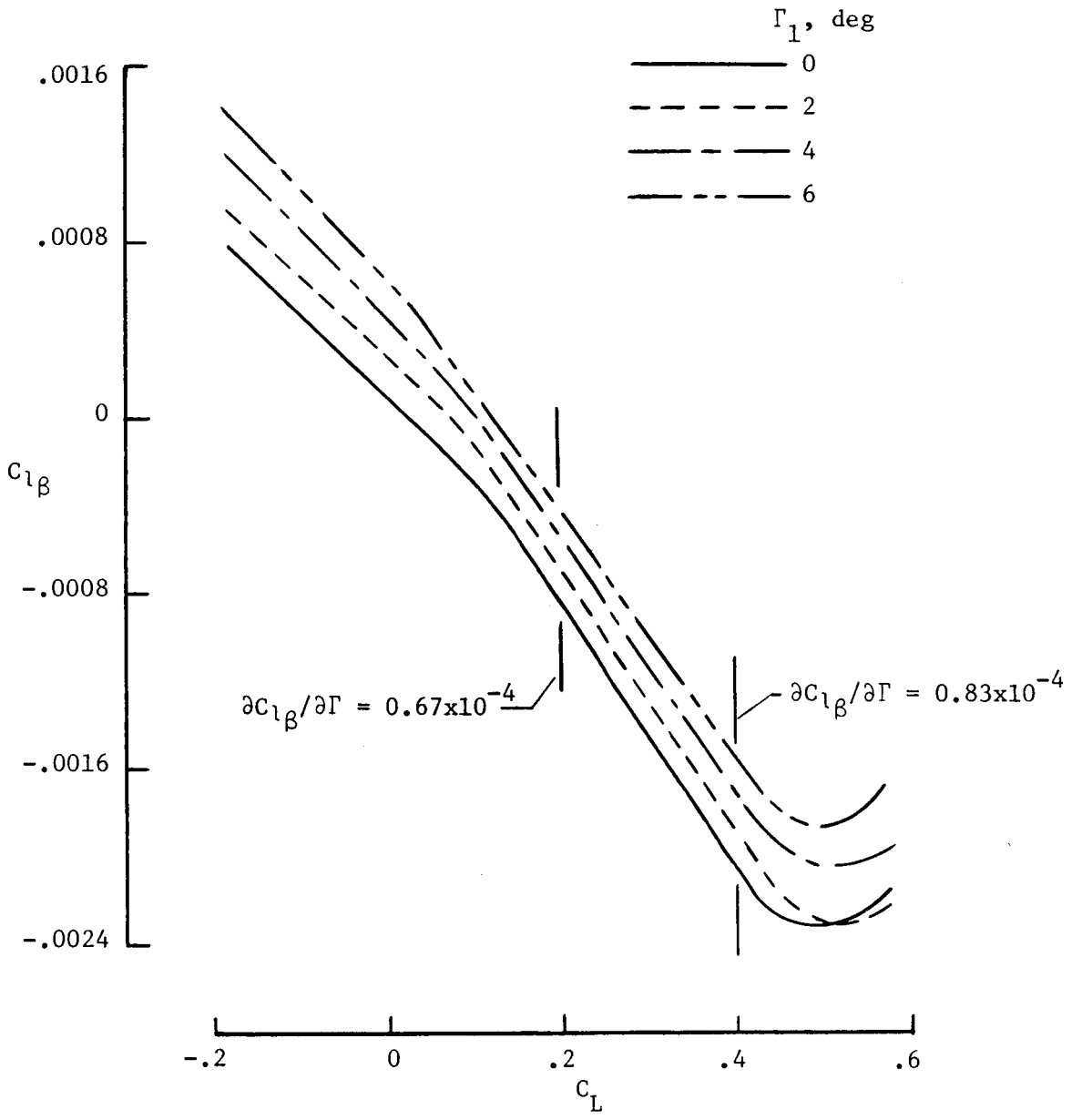

(a) Γ_1 varied, $\Gamma_2 = 0^\circ$.

Figure 21.- Effect of geometric anhedral on C_{l_β}.

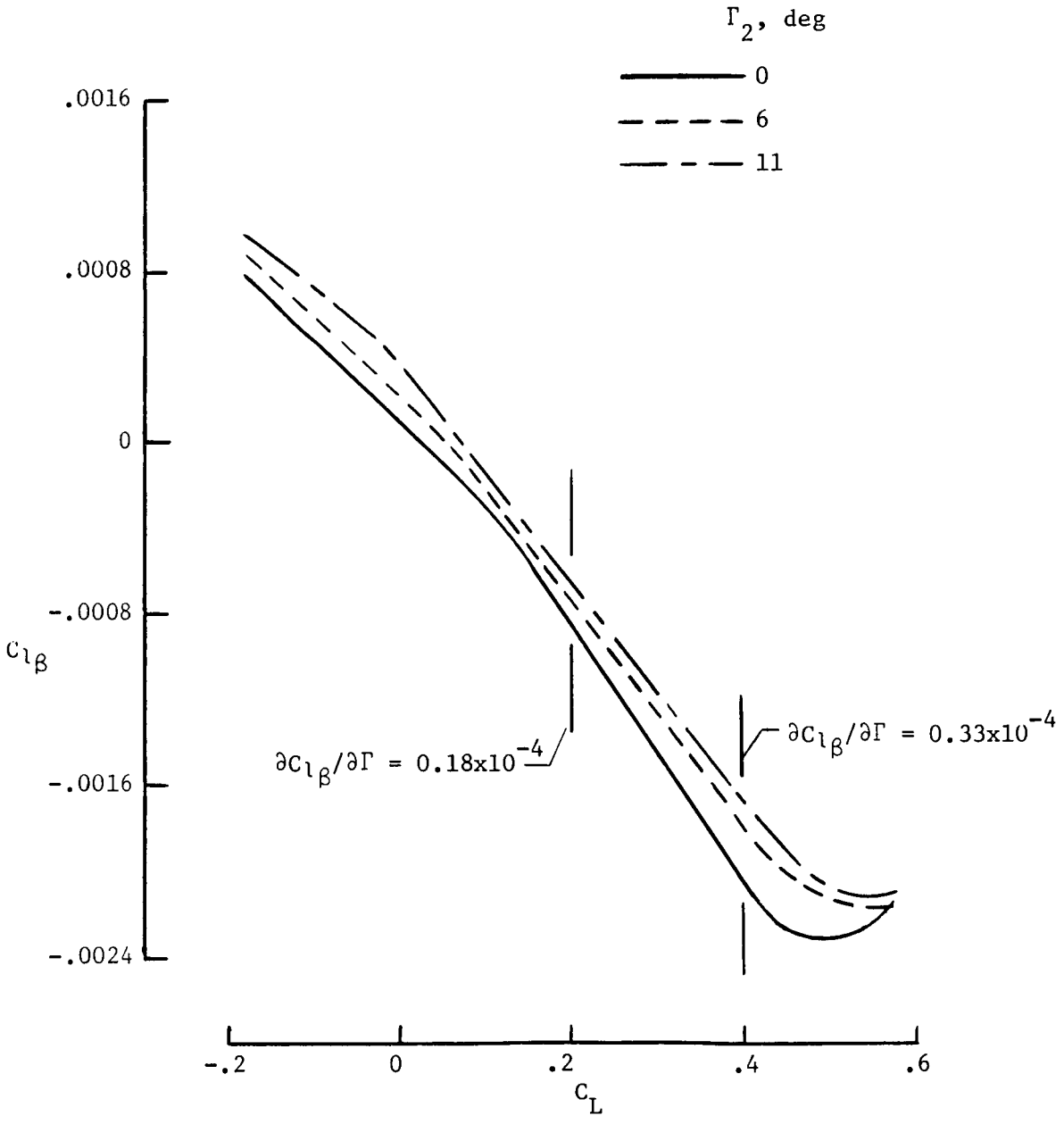

(b) $\Gamma_1 = 0^o$, Γ_2 varied.

Figure 21.- Concluded.

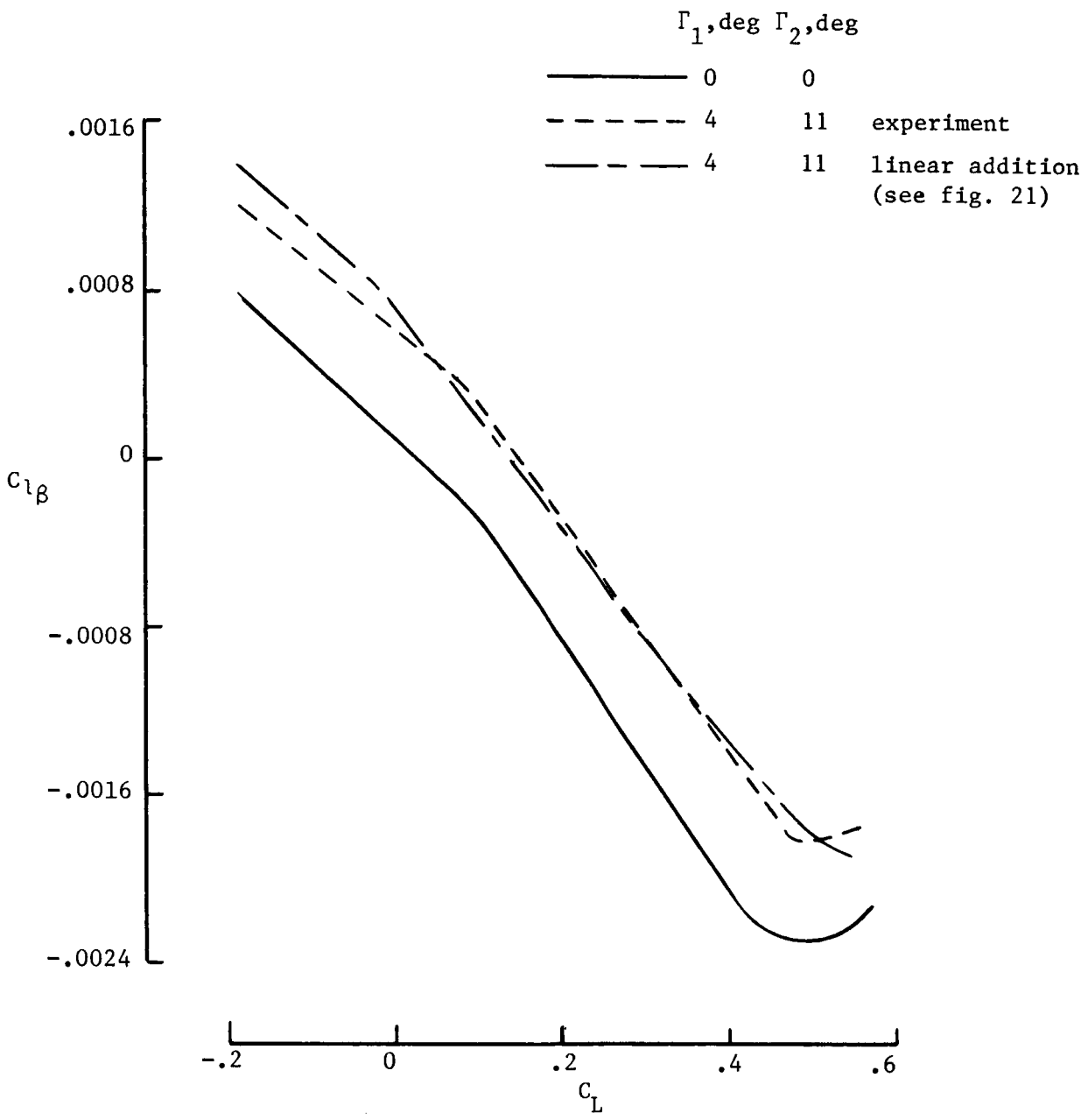

Figure 22.- Effect of geometric anhedral, Γ_1 and Γ_2 in combination, on C_{l_β}.

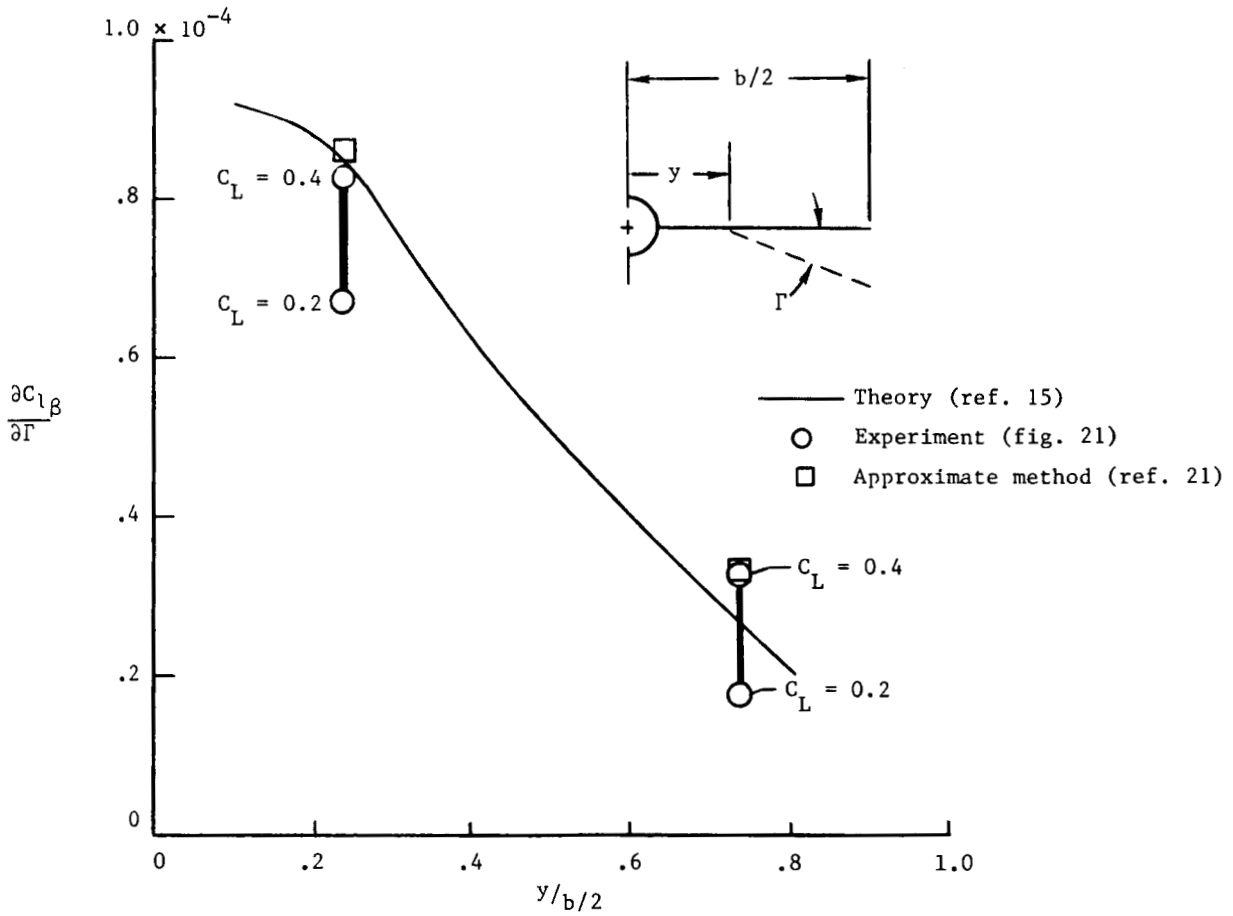

Figure 23.- Values for $\partial C_{l_\beta}/\partial \Gamma$ obtained by inclusion of additional geometric anhedral at span station $\frac{y}{b/2}$.

APPENDIX A

EFFECT OF GEOMETRIC ANHEDRAL ON C_{l_β}

The following simple analysis is intended to illustrate the effect on C_{l_β} of increasing the geometric anhedral of the configuration reported herein. The analysis assumes that the wing-tip clearance remains unchanged, as would be required for the case wherein the landing gear length is held constant.

Consider the wing semispan sketched in figure A1. The spanwise location of the anhedral breaks, and the corresponding anhedral angles define the change in vertical height of the wing tip (Δz_{tip}) as

$$\Delta z_{tip} = \Gamma_i(b/2 - y_i) + \Gamma_o(b/2 - y_o) \tag{A1}$$

where the subscripts i and o refer to the values associated with assumed inboard and outboard locations, respectively. Requiring $\Delta z_{tip} = 0$ and solving for Γ_o yields

$$\Gamma_o = -\Gamma_i \frac{\left(1 - \frac{y_i}{b/2}\right)}{\left(1 - \frac{y_o}{b/2}\right)} \tag{A2}$$

As shown in the body of this report (see figs. 21 and 22), the increment in C_{l_β} resulting from Γ_i and Γ_o may be determined by linear combination, therefore

$$\Delta C_{l_\beta} = \frac{\partial C_{l_\beta}}{\partial \Gamma_i} \times \Gamma_i + \frac{\partial C_{l_\beta}}{\partial \Gamma_o} \times \Gamma_o \tag{A3}$$

Substituting equation (A2) into equation (A3) yields

$$\Delta C_{l_\beta} = \left[\frac{\partial C_{l_\beta}}{\partial \Gamma_i} - \left(\frac{1 - \frac{y_i}{b/2}}{1 - \frac{y_o}{b/2}}\right) \times \frac{\partial C_{l_\beta}}{\partial \Gamma_o}\right] \Gamma_i \tag{A4}$$

APPENDIX A

Evaluation of equation (A4) shows that, for the variation of $\partial C_{l_\beta}/\partial\Gamma$ presented in figure 23, maintaining constant wing-tip clearance would limit the favorable increments in C_{l_β} to negligible values. For example, consider the result for the spanwise location of anhedral breaks tested on the present configuration. At span locations $\frac{y_i}{b/2} = 0.234$ and 0.736, the theoretical results of figure 23 show $\partial C_{l_\beta}/\partial\Gamma_i = 0.85 \times 10^{-4}$ and $\partial C_{l_\beta}/\partial\Gamma_o = 0.27 \times 10^{-4}$. Assuming the anhedral at the inboard location is increased by 5° (with no constraint on wing-tip clearance), the increment in C_{l_β} for this condition would be $\Delta C_{l_\beta} = 4.25 \times 10^{-4}$. However, constraining the change in wing-tip clearance to zero and assuming the value of $\Delta C_{l_\beta}/\partial\Gamma_o$ applicable for increased dihedral angles, the increment in C_{l_β} would be only 0.33×10^{-4}.

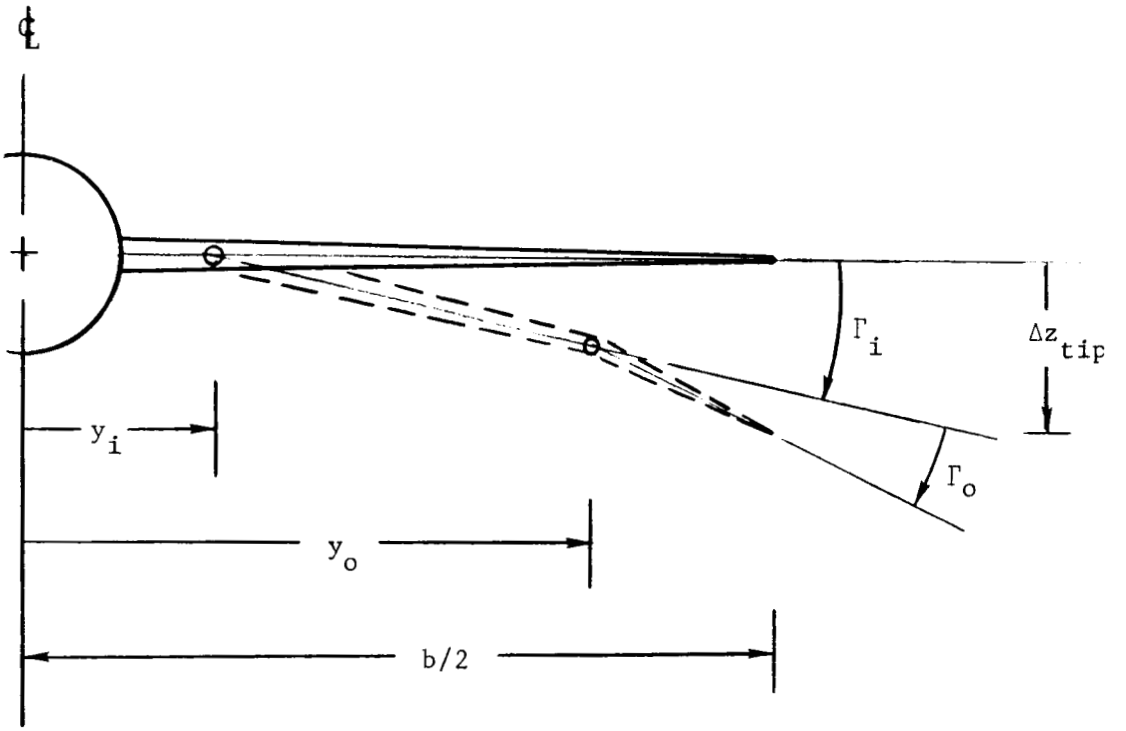

$$\Delta z_{tip} = \Gamma_i \left(\frac{b}{2} - y_i\right) + \Gamma_o \left(\frac{b}{2} - y_o\right)$$

for $\Delta z_{tip} = 0$

$$\Gamma_o = -\Gamma_i \frac{1 - \frac{y_i}{b/2}}{1 - \frac{y_o}{b/2}}$$

Figure A1.- Geometric relationship of anhedral angles and wingtip height.

APPENDIX B

DATA SUPPLEMENT

The symbols used in the data tabulation are defined as follows:

ALPHA	angle of attack, deg
BETA	angle of sideslip, deg
CD	drag-force coefficient; stability axis
CL	lift-force coefficient; stability axis
CM	pitching-moment coefficient; stability axis
CRM	rolling-moment coefficient; body axis
CY	side-force coefficient; body axis
CYM	yawing-moment coefficient; body axis

APPENDIX B

TABLE B1.- TEST PROGRAM

Run	β, deg	$\delta_{L.E.}$, deg	Γ_1, deg	Γ_2, deg
1	0	0	0	0
2	5	↓	↓	↓
3	-5	↓	↓	↓
4	-5	30	↓	↓
5	5	↓	↓	↓
6	0	↓	↓	↓
12	0	16-50	↓	↓
13	5	↓	↓	↓
14	-5	↓	↓	↓
18	0	↓	6	↓
19	5	↓	↓	↓
20	-5	↓	↓	↓
21	-5	↓	4	↓
22	5	↓	↓	↓
23	0	↓	↓	↓
24	0	↓	↓	11
25	5	↓	↓	↓
26	-5	↓	↓	↓
27	-5	↓	2	0
28	5	↓	↓	↓
29	0	↓	↓	↓
30	0	↓	0	11
31	5	↓	↓	↓
32	-5	↓	↓	↓
33	-5	↓	↓	6
34	5	↓	↓	↓
35	0	↓	↓	↓
39	0	16-50 unfaired	↓	0

APPENDIX B

TABLE B2.- TABULATED DATA

NASA LANGLEY 7 X 10 HIGH SPEED TUNNEL

TEST 59 RUN 1

BETA	ALPHA	CL	CD	CM	CRM	CYM	CY
-.06	.17	.0906	.0110	.0128	-.0003	-.0003	.0009
-.08	-5.64	-.1296	.0189	.0078	-.0010	-.0005	.0018
-.08	-3.72	-.0493	.0118	.0088	-.0006	-.0005	.0015
-.07	-1.72	.0256	.0097	.0098	-.0003	-.0003	.0010
-.06	.19	.0939	.0110	.0131	.0003	-.0003	.0014
-.06	2.25	.1700	.0156	.0160	.0000	-.0002	.0015
-.05	4.25	.2521	.0260	.0160	.0001	-.0000	.0006
-.05	6.34	.3456	.0442	.0198	.0003	.0002	.0008
-.04	8.57	.4633	.0754	.0290	.0008	.0005	.0025
-.04	10.51	.5700	.1142	.0441	.0001	.0011	.0034
-.03	12.69	.6907	.1667	.0625	-.0001	.0014	.0048
-.03	14.74	.8019	.2251	.0850	-.0008	.0016	.0064
-.03	15.10	.8195	.2356	.0893	-.0007	.0016	.0065
-.07	.19	.0978	.0114	.0133	-.0001	-.0002	.0025

TEST 59 RUN 2

BETA	ALPHA	CL	CD	CM	CRM	CYM	CY
4.90	.15	.0926	.0107	.0130	-.0031	.0001	-.0101
4.92	-5.72	-.1304	.0193	.0054	.0031	-.0004	-.0113
4.91	-3.75	-.0468	.0117	.0074	.0020	-.0001	-.0100
4.91	-1.75	.0268	.0095	.0092	-.0006	.0001	-.0094
4.90	.17	.0956	.0108	.0134	-.0032	.0002	-.0099
4.88	2.23	.1706	.0158	.0159	-.0048	.0004	-.0099
4.86	4.24	.2568	.0267	.0181	-.0057	.0012	-.0116
4.81	6.33	.3497	.0457	.0229	-.0087	.0033	-.0069
4.77	8.43	.4559	.0742	.0329	-.0111	.0064	-.0048
4.72	10.45	.5507	.1087	.0462	-.0137	.0083	-.0024
4.67	12.67	.6726	.1612	.0655	-.0179	.0089	-.0007
4.61	14.76	.7923	.2228	.0877	-.0209	.0094	-.0010
4.60	15.01	.8022	.2295	.0905	-.0216	.0095	-.0000
4.90	.15	.0996	.0112	.0136	-.0031	.0001	-.0093

TEST 59 RUN 3

BETA	ALPHA	CL	CD	CM	CRM	CYM	CY
-5.02	.24	.0918	.0113	.0123	.0023	-.0005	.0100
-5.08	-5.63	-.1305	.0195	.0052	-.0049	-.0006	.0136
-5.06	-3.64	-.0474	.0122	.0077	-.0028	-.0008	.0120
-5.05	-1.66	.0246	.0102	.0094	-.0001	-.0007	.0106
-5.02	.26	.0921	.0113	.0121	.0024	-.0006	.0098
-4.99	2.32	.1677	.0161	.0147	.0035	-.0005	.0102
-4.96	4.36	.2520	.0270	.0166	.0053	-.0005	.0104
-4.91	6.42	.3476	.0459	.0224	.0065	-.0026	.0078
-4.85	8.54	.4481	.0741	.0318	.0092	-.0043	.0060
-4.79	10.57	.5554	.1111	.0444	.0119	-.0063	.0042
-4.73	12.78	.6732	.1634	.0629	.0143	-.0060	.0051
-4.66	14.86	.7961	.2248	.0839	.0198	-.0056	.0037
-4.65	15.21	.8150	.2359	.0904	.0196	-.0054	.0043
-5.02	.26	.0941	.0116	.0126	.0022	-.0007	.0103

TEST 59 RUN 4

BETA	ALPHA	CL	CD	CM	CRM	CYM	CY
-5.03	.20	.0751	.0141	.0023	.0003	.0008	.0146
-5.10	-5.71	-.1607	.0336	-.0140	-.0061	.0008	.0250
-5.08	-3.72	-.0777	.0221	-.0061	-.0037	.0009	.0213
-5.06	-1.70	.0028	.0158	-.0014	-.0017	.0011	.0172
-5.03	.23	.0784	.0145	.0024	.0001	.0008	.0159
-5.00	2.32	.1564	.0164	.0054	.0031	.0004	.0142
-4.96	4.30	.2282	.0217	.0092	.0053	.0000	.0149
-4.92	6.37	.3049	.0317	.0110	.0073	-.0003	.0162
-4.88	8.45	.3870	.0471	.0130	.0072	.0014	.0158
-4.83	10.37	.4565	.0655	.0173	.0080	.0015	.0129
-4.77	12.53	.5470	.0956	.0237	.0072	.0017	.0129
-4.71	14.51	.6230	.1285	.0323	.0081	.0027	.0150
-4.70	14.65	.6366	.1348	.0333	.0086	.0029	.0143
-5.04	.24	.0886	.0150	.0027	.0003	.0009	.0174

TABLE B2.- Continued

NASA LANGLEY 7 X 10 HIGH SPEED TUNNEL

TEST 59 RUN 5

BETA	ALPHA	CL	CD	CM	CRM	CYM	CY
4.91	.11	.0780	.0140	.0026	-.0009	-.0017	-.0133
4.93	-5.79	-.1598	.0336	-.0140	.0048	-.0020	-.0220
4.93	-3.82	-.0789	.0221	-.0066	.0025	-.0019	-.0181
4.92	-1.80	.0026	.0158	-.0006	.0009	-.0019	-.0151
4.91	.14	.0784	.0137	.0027	-.0007	-.0017	-.0138
4.89	2.21	.1543	.0155	.0060	-.0034	-.0011	-.0119
4.87	4.20	.2264	.0209	.0089	-.0050	-.0011	-.0134
4.83	6.27	.2987	.0290	.0121	-.0065	-.0000	-.0128
4.80	8.30	.3754	.0428	.0154	-.0081	-.0003	-.0108
4.76	10.27	.4534	.0626	.0164	-.0102	-.0006	-.0110
4.71	12.47	.5450	.0939	.0223	-.0089	-.0008	-.0097
4.65	14.64	.6223	.1284	.0332	-.0107	.0004	-.0101
4.91	.12	.0780	.0141	.0022	-.0010	-.0018	-.0134

TEST 59 RUN 6

BETA	ALPHA	CL	CD	CM	CRM	CYM	CY
-.06	.11	.0738	.0137	.0027	-.0002	-.0003	.0015
-.08	-5.76	-.1653	.0340	-.0114	-.0010	-.0006	.0029
-.08	-3.79	-.0854	.0226	-.0042	-.0008	-.0004	.0026
-.07	-1.78	-.0013	.0156	.0001	-.0002	-.0004	.0014
-.06	.13	.0750	.0135	.0023	-.0002	-.0003	.0015
-.06	2.20	.1516	.0153	.0058	.0000	-.0004	.0016
-.05	4.19	.2224	.0206	.0084	.0010	-.0004	.0019
-.04	6.24	.2945	.0296	.0107	.0013	-.0005	.0022
-.04	8.31	.3744	.0439	.0131	.0005	.0002	.0016
-.04	10.24	.4488	.0627	.0165	-.0011	.0010	.0033
-.04	12.36	.5316	.0897	.0227	-.0012	.0022	.0064
-.03	14.68	.6338	.1318	.0296	-.0030	.0033	.0031
-.06	.11	.0750	.0140	.0033	-.0001	-.0003	.0015

TEST 59 RUN 12

BETA	ALPHA	CL	CD	CM	CRM	CYM	CY
-.06	.11	.0632	.0138	.0101	.0009	-.0001	.0011
-.08	-5.75	-.1733	.0347	-.0038	-.0002	.0001	.0012
-.08	-3.81	-.0968	.0235	.0036	.0002	.0004	.0011
-.07	-1.78	-.0151	.0164	.0091	.0007	.0002	.0007
-.06	.12	.0629	.0135	.0100	.0007	-.0001	.0008
-.06	2.18	.1432	.0149	.0089	.0009	-.0002	.0019
-.05	4.17	.2168	.0190	.0105	.0006	-.0003	.0019
-.05	6.23	.2905	.0269	.0123	.0011	-.0002	.0023
-.04	8.28	.3703	.0399	.0127	.0009	.0001	.0034
-.04	10.21	.4366	.0552	.0166	.0002	.0014	.0060
-.03	12.33	.5145	.0773	.0227	.0003	.0007	.0076
-.04	12.32	.5144	.0776	.0228	-.0000	.0006	.0085
-.02	14.64	.6022	.1138	.0327	.0012	.0003	.0078
-.06	.12	.0640	.0140	.0100	.0011	-.0001	.0008

TEST 59 RUN 13

BETA	ALPHA	CL	CD	CM	CRM	CYM	CY
4.90	.10	.0651	.0142	.0095	.0004	.0001	-.0136
4.93	-5.67	-.1744	.0350	-.0066	.0040	-.0012	-.0199
4.93	-3.90	-.0967	.0237	.0016	.0027	-.0013	-.0165
4.92	-1.89	-.0137	.0167	.0070	.0011	-.0010	-.0135
4.90	.06	.0620	.0141	.0099	.0009	.0001	-.0140
4.88	2.09	.1410	.0146	.0103	-.0022	.0002	-.0131
4.86	4.11	.2157	.0187	.0113	-.0050	-.0000	-.0140
4.83	6.15	.2932	.0267	.0116	-.0064	.0008	-.0149
4.80	8.20	.3621	.0381	.0143	-.0087	.0007	-.0123
4.76	10.16	.4393	.0555	.0170	-.0110	-.0001	-.0108
4.71	12.30	.5243	.0823	.0237	-.0111	-.0011	-.0066
4.65	14.62	.6164	.1188	.0352	-.0122	-.0019	.0015
4.90	.01	.0620	.0143	.0097	.0007	.0001	-.0131

TABLE B2.- Continued

NASA LANGLEY 7 X 10 HIGH SPEED TUNNEL

TEST 59 RUN 14

BETA	ALPHA	CL	CD	CM	CRM	CYM	CY
-5.03	.20	.0656	.0143	.0084	.0005	-.0001	.0135
-5.09	-5.73	-.1703	.0346	-.0067	-.0036	.0012	.0206
-5.08	-3.75	-.0906	.0234	.0009	-.0020	.0013	.0168
-5.06	-1.74	-.0113	.0166	.0066	-.0005	.0008	.0142
-5.03	.18	.0649	.0141	.0082	.0006	-.0001	.0133
-5.00	2.26	.1455	.0154	.0087	.0028	-.0006	.0129
-4.96	4.28	.2178	.0196	.0108	.0051	-.0007	.0142
-4.92	6.31	.2934	.0280	.0122	.0068	-.0007	.0158
-4.87	8.37	.3678	.0404	.0137	.0088	-.0004	.0158
-4.82	10.31	.4386	.0560	.0167	.0110	-.0001	.0127
-4.76	12.44	.5202	.0813	.0232	.0103	.0008	.0117
-4.69	14.81	.6289	.1241	.0331	.0066	.0005	.0095
-5.03	.19	.0670	.0144	.0087	.0001	-.0001	.0142

TEST 59 RUN 18

BETA	ALPHA	CL	CD	CM	CRM	CYM	CY
-.07	.13	.0686	.0145	.0103	.0002	.0001	.0014
-.09	-5.70	-.1606	.0344	-.0027	-.0003	.0005	.0022
-.08	-3.76	-.0811	.0237	.0036	.0006	.0007	.0014
-.07	-1.77	-.0034	.0171	.0083	.0006	.0006	.0009
-.07	.18	.0737	.0146	.0101	.0003	.0001	.0020
-.06	2.23	.1539	.0163	.0097	.0006	-.0001	.0025
-.05	4.22	.2262	.0210	.0116	.0004	-.0002	.0029
-.05	6.26	.2987	.0292	.0131	.0006	-.0003	.0044
-.04	8.30	.3773	.0426	.0136	.0007	.0001	.0044
-.04	10.24	.4445	.0583	.0185	.0002	.0013	.0075
-.04	12.37	.5186	.0806	.0253	-.0000	.0009	.0082
-.03	14.63	.6026	.1142	.0344	.0001	-.0002	.0089
-.07	.15	.0791	.0153	.0103	.0003	.0001	.0032

TEST 59 RUN 19

BETA	ALPHA	CL	CD	CM	CRM	CYM	CY
4.90	.16	.0676	.0145	.0099	.0030	.0005	-.0166
4.93	-5.79	-.1655	.0344	-.0050	.0067	-.0007	-.0242
4.93	-3.82	-.0865	.0234	.0012	.0052	-.0008	-.0205
4.92	-1.81	-.0085	.0169	.0069	.0040	-.0004	-.0174
4.90	.10	.0651	.0146	.0099	.0028	.0005	-.0159
4.88	2.18	.1429	.0156	.0112	.0000	.0009	-.0155
4.86	4.19	.2160	.0196	.0125	-.0025	.0009	-.0160
4.83	6.23	.2906	.0274	.0125	-.0044	.0016	-.0170
4.80	8.27	.3605	.0387	.0166	-.0065	.0012	-.0164
4.76	10.23	.4359	.0558	.0204	-.0089	.0005	-.0142
4.71	12.35	.5141	.0811	.0266	-.0097	-.0011	-.0094
4.65	14.61	.6136	.1196	.0364	-.0087	-.0016	-.0029
4.90	.10	.0650	.0146	.0098	.0032	.0006	-.0168

TEST 59 RUN 20

BETA	ALPHA	CL	CD	CM	CRM	CYM	CY
-5.03	.18	.0616	.0142	.0085	-.0019	-.0002	.0136
-5.09	-5.71	-.1693	.0348	-.0050	-.0055	.0016	.0211
-5.08	-3.72	-.0903	.0236	.0014	-.0040	.0016	.0170
-5.06	-1.73	-.0140	.0170	.0067	-.0032	.0008	.0149
-5.03	.21	.0645	.0144	.0086	-.0015	-.0001	.0140
-5.00	2.25	.1414	.0155	.0094	.0012	-.0007	.0132
-4.96	4.27	.2124	.0196	.0116	.0031	-.0009	.0141
-4.92	6.31	.2850	.0274	.0130	.0043	-.0011	.0162
-4.88	8.36	.3595	.0392	.0160	.0058	-.0006	.0173
-4.82	10.31	.4330	.0558	.0193	.0088	-.0009	.0144
-4.76	12.46	.5129	.0800	.0251	.0084	.0001	.0128
-4.69	14.78	.6129	.1193	.0325	.0051	.0013	.0103
-5.03	.18	.0601	.0144	.0084	-.0016	-.0001	.0130

APPENDIX B

TABLE B2.- Continued

NASA LANGLEY 7 X 10 HIGH SPEED TUNNEL

TEST 59 RUN 21

BETA	ALPHA	CL	CD	CM	CRM	CYM	CY
-5.03	.19	.0675	.0142	.0063	-.0014	-.0001	.0151
-5.10	-5.70	-.1617	.0337	-.0065	-.0044	.0017	.0220
-5.08	-3.71	-.0826	.0228	.0008	-.0035	.0018	.0178
-5.06	-1.70	-.0032	.0164	.0061	-.0022	.0009	.0157
-5.03	.21	.0713	.0144	.0081	-.0011	-.0001	.0157
-5.00	2.26	.1518	.0161	.0092	.0014	-.0007	.0150
-4.96	4.28	.2250	.0207	.0114	.0035	-.0008	.0169
-4.92	6.31	.2973	.0288	.0119	.0048	-.0010	.0182
-4.88	8.42	.3740	.0418	.0157	.0064	-.0005	.0196
-4.82	10.34	.4475	.0585	.0181	.0098	-.0005	.0152
-4.76	12.48	.5272	.0835	.0242	.0095	.0004	.0128
-4.69	14.82	.6309	.1251	.0333	.0062	.0009	.0101
-5.03	.22	.0774	.0148	.0081	-.0009	.0001	.0165

TEST 59 RUN 22

BETA	ALPHA	CL	CD	CM	CRM	CYM	CY
4.90	.11	.0688	.0143	.0093	.0017	.0003	-.0145
4.93	-5.77	-.1639	.0337	-.0058	.0058	-.0010	-.0217
4.93	-3.79	-.0852	.0231	.0019	.0040	-.0011	-.0179
4.92	-1.78	-.0030	.0162	.0070	.0028	-.0006	-.0156
4.90	.14	.0686	.0141	.0090	.0019	.0004	-.0146
4.88	2.21	.1482	.0153	.0104	-.0009	.0007	-.0139
4.86	4.25	.2251	.0198	.0121	-.0033	.0007	-.0152
4.83	6.27	.2971	.0276	.0121	-.0056	.0012	-.0146
4.80	8.32	.3711	.0397	.0160	-.0074	.0012	-.0157
4.76	10.30	.4451	.0576	.0183	-.0095	.0007	-.0121
4.71	12.40	.5232	.0836	.0253	-.0098	-.0009	-.0085
4.65	14.62	.6118	.1185	.0371	-.0109	-.0019	-.0013
4.90	.15	.0733	.0144	.0101	.0015	.0003	-.0140

TEST 59 RUN 23

BETA	ALPHA	CL	CD	CM	CRM	CYM	CY
-.06	.11	.0620	.0134	.0092	.0005	.0001	-.0000
-.08	-5.76	-.1710	.0341	-.0026	-.0002	.0004	.0004
-.08	-3.79	-.0935	.0230	.0042	.0003	.0004	.0000
-.07	-1.78	-.0125	.0162	.0087	.0005	.0003	.0003
-.06	.14	.0640	.0137	.0092	.0007	.0002	.0003
-.06	2.22	.1460	.0146	.0091	.0007	-.0001	.0004
-.05	4.18	.2165	.0188	.0108	.0004	-.0001	.0008
-.04	6.22	.2858	.0264	.0124	.0011	-.0003	.0010
-.04	8.33	.3708	.0397	.0133	.0007	.0002	.0021
-.04	10.30	.4377	.0550	.0177	.0002	.0015	.0041
-.03	12.33	.5078	.0763	.0239	-.0001	.0004	.0057
-.02	14.62	.5914	.1102	.0336	.0015	-.0004	.0028
-.06	.12	.0635	.0132	.0092	-.0000	.0001	.0005

TEST 59 RUN 24

BETA	ALPHA	CL	CD	CM	CRM	CYM	CY
-.06	.13	.0674	.0139	.0096	.0006	.0000	.0009
-.08	-5.70	-.1557	.0320	-.0060	-.0004	.0001	.0014
-.08	-3.77	-.0843	.0224	.0027	-.0002	.0001	.0019
-.07	-1.78	-.0071	.0163	.0078	.0003	.0002	.0013
-.07	.13	.0693	.0138	.0094	.0005	.0000	.0011
-.06	2.21	.1505	.0153	.0095	.0002	-.0003	.0025
-.05	4.18	.2189	.0195	.0110	.0005	-.0003	.0022
-.05	6.25	.2943	.0276	.0144	.0006	-.0002	.0025
-.04	8.30	.3686	.0409	.0151	.0006	.0001	.0036
-.04	10.22	.4370	.0565	.0199	.0001	.0013	.0062
-.03	12.33	.5085	.0782	.0270	-.0005	.0006	.0075
-.02	14.63	.5960	.1113	.0371	.0005	-.0010	.0076
-.07	.15	.0742	.0140	.0101	.0005	.0001	.0022

TABLE B2.- Continued

NASA LANGLEY 7 X 10 HIGH SPEED TUNNEL

TEST 59 RUN 25

BETA	ALPHA	CL	CD	CM	CRM	CYM	CY
4.90	.10	.0637	.0138	.0088	.0037	.0017	-.0190
4.93	-5.78	-.1591	.0325	-.0082	.0061	-.0006	-.0228
4.93	-3.83	-.0852	.0226	-.0001	.0052	-.0006	-.0194
4.92	-1.82	-.0076	.0163	.0062	.0043	.0004	-.0181
4.90	.09	.0636	.0137	.0090	.0036	.0019	-.0191
4.88	2.16	.1421	.0149	.0111	.0011	.0020	-.0179
4.86	4.16	.2145	.0188	.0130	-.0018	.0015	-.0185
4.83	6.24	.2900	.0272	.0133	-.0036	.0026	-.0185
4.80	8.28	.3629	.0392	.0161	-.0063	.0024	-.0171
4.76	10.28	.4383	.0566	.0222	-.0081	.0019	-.0161
4.71	12.35	.5120	.0815	.0280	-.0075	.0008	-.0141
4.65	14.60	.6003	.1163	.0409	-.0092	-.0001	-.0052
4.90	.09	.0658	.0139	.0090	.0031	.0017	-.0179

TEST 59 RUN 26

BETA	ALPHA	CL	CD	CM	CRM	CYM	CY
-5.03	.19	.0635	.0138	.0081	-.0024	-.0016	.0171
-5.09	-5.70	-.1617	.0327	-.0100	-.0053	.0010	.0225
-5.08	-3.72	-.0857	.0225	-.0004	-.0040	.0010	.0185
-5.05	-1.71	-.0088	.0161	.0051	-.0027	.0000	.0168
-5.03	.20	.0616	.0138	.0080	-.0022	-.0015	.0168
-5.00	2.26	.1403	.0148	.0099	-.0000	-.0019	.0160
-4.96	4.30	.2138	.0194	.0114	.0026	-.0019	.0166
-4.92	6.31	.2870	.0273	.0136	.0040	-.0020	.0175
-4.88	8.38	.3613	.0399	.0172	.0053	-.0016	.0201
-4.81	10.44	.4369	.0569	.0209	.0082	-.0019	.0154
-4.76	12.46	.5092	.0798	.0271	.0091	-.0016	.0139
-4.69	14.79	.6122	.1194	.0370	.0062	.0001	.0089
-5.03	.21	.0654	.0139	.0087	-.0025	-.0016	.0170

TEST 59 RUN 27

BETA	ALPHA	CL	CD	CM	CRM	CYM	CY
-5.03	.19	.0703	.0141	.0070	-.0008	-.0001	.0131
-5.09	-5.71	-.1632	.0339	-.0075	-.0046	.0015	.0210
-5.08	-3.73	-.0860	.0230	.0010	-.0028	.0016	.0159
-5.06	-1.71	-.0045	.0164	.0062	-.0015	.0010	.0144
-5.03	.24	.0740	.0142	.0077	-.0004	-.0003	.0131
-5.00	2.27	.1531	.0156	.0086	.0015	-.0005	.0139
-4.96	4.30	.2264	.0202	.0102	.0040	-.0007	.0142
-4.92	6.33	.3017	.0289	.0121	.0050	-.0006	.0165
-4.88	8.41	.3770	.0417	.0137	.0070	-.0002	.0166
-4.82	10.34	.4482	.0577	.0161	.0093	-.0004	.0129
-4.76	12.49	.5279	.0830	.0225	.0101	.0001	.0106
-4.69	14.83	.6362	.1255	.0330	.0062	.0004	.0081
-5.03	.22	.0775	.0145	.0077	-.0005	-.0001	.0139

TEST 59 RUN 28

BETA	ALPHA	CL	CD	CM	CRM	CYM	CY
4.90	.10	.0668	.0141	.0091	.0013	.0003	-.0140
4.93	-5.80	-.1659	.0341	-.0066	.0044	-.0010	-.0202
4.92	-3.84	-.0884	.0234	.0016	.0033	-.0012	-.0164
4.92	-1.84	-.0076	.0168	.0065	.0019	-.0007	-.0143
4.90	.09	.0673	.0141	.0088	.0015	.0003	-.0141
4.88	2.17	.1478	.0151	.0104	-.0013	.0006	-.0135
4.86	4.17	.2190	.0189	.0110	-.0044	.0004	-.0142
4.83	6.22	.2981	.0271	.0115	-.0065	.0008	-.0146
4.80	8.27	.3698	.0389	.0137	-.0088	.0008	-.0149
4.76	10.23	.4433	.0566	.0157	-.0113	.0005	-.0113
4.71	12.39	.5234	.0826	.0224	-.0112	-.0008	-.0088
4.65	14.62	.6111	.1174	.0353	-.0127	-.0013	-.0009
4.90	.09	.0672	.0141	.0089	.0010	.0002	-.0142

TABLE B2.- Continued

NASA LANGLEY 7 X 10 HIGH SPEED TUNNEL

TEST 59 RUN 29

BETA	ALPHA	CL	CD	CM	CRM	CYM	CY
-.06	.12	.0656	.0138	.0091	.0007	-.0001	-.0001
-.08	-5.76	-.1721	.0345	-.0041	-.0004	.0003	.0008
-.08	-3.80	-.0921	.0233	.0037	-.0005	.0002	.0009
-.07	-1.78	-.0116	.0164	.0076	.0007	.0002	.0002
-.06	.14	.0668	.0138	.0097	.0007	-.0000	.0007
-.06	2.18	.1474	.0147	.0079	.0003	-.0001	.0010
-.05	4.20	.2193	.0189	.0094	.0002	-.0003	.0006
-.04	6.22	.2925	.0267	.0109	.0001	-.0004	.0018
-.04	8.29	.3692	.0397	.0114	.0001	-.0000	.0024
-.04	10.24	.4393	.0555	.0157	-.0006	.0013	.0051
-.03	12.40	.5176	.0784	.0220	-.0009	.0003	.0070
-.02	14.63	.5997	.1116	.0310	.0002	-.0006	.0061
-.06	.12	.0641	.0138	.0089	.0006	-.0001	-.0002

TEST 59 RUN 30

BETA	ALPHA	CL	CD	CM	CRM	CYM	CY
-.06	.12	.0659	.0136	.0088	.0002	-.0001	.0009
-.08	-5.73	-.1628	.0333	-.0085	-.0005	.0002	.0015
-.08	-3.78	-.0896	.0230	.0019	.0000	.0002	.0011
-.07	-1.77	-.0084	.0163	.0071	.0007	.0004	.0005
-.06	.15	.0688	.0138	.0090	.0006	-.0000	.0010
-.06	2.20	.1489	.0148	.0082	.0006	-.0002	.0012
-.05	4.26	.2213	.0194	.0101	.0003	-.0003	.0021
-.05	6.25	.2925	.0272	.0131	.0007	-.0001	.0027
-.04	8.30	.3716	.0408	.0127	.0011	.0001	.0023
-.04	10.25	.4395	.0566	.0179	.0002	.0013	.0057
-.03	12.37	.5129	.0781	.0246	-.0002	.0006	.0056
-.02	14.64	.6013	.1132	.0337	.0007	-.0011	.0064
-.06	.15	.0728	.0138	.0102	-.0003	-.0001	.0013

TEST 59 RUN 31

BETA	ALPHA	CL	CD	CM	CRM	CYM	CY
4.90	.09	.0648	.0136	.0081	.0019	.0014	-.0170
4.93	-5.80	-.1613	.0329	-.0097	.0048	-.0006	-.0212
4.92	-3.81	-.0853	.0225	-.0009	.0038	-.0007	-.0182
4.92	-1.79	-.0060	.0160	.0054	.0025	.0001	-.0169
4.90	.15	.0692	.0136	.0088	.0021	.0014	-.0171
4.88	2.18	.1462	.0146	.0096	-.0012	.0013	-.0160
4.86	4.21	.2191	.0186	.0112	-.0038	.0011	-.0167
4.83	6.24	.2950	.0270	.0121	-.0051	.0018	-.0178
4.80	8.32	.3712	.0396	.0153	-.0078	.0016	-.0164
4.76	10.27	.4419	.0569	.0188	-.0090	.0015	-.0148
4.71	12.44	.5249	.0843	.0265	-.0096	.0001	-.0109
4.65	14.63	.6105	.1183	.0377	-.0116	-.0008	-.0016
4.90	.11	.0686	.0136	.0081	.0021	.0013	-.0177

TEST 59 RUN 32

BETA	ALPHA	CL	CD	CM	CRM	CYM	CY
-5.03	.20	.0666	.0140	.0068	-.0010	-.0011	.0159
-5.09	-5.71	-.1613	.0329	-.0107	-.0049	.0008	.0216
-5.08	-3.76	-.0859	.0226	-.0015	-.0033	.0009	.0177
-5.05	-1.72	-.0075	.0161	.0046	-.0015	.0002	.0156
-5.03	.18	.0662	.0138	.0070	-.0009	-.0010	.0157
-5.00	2.26	.1463	.0151	.0088	.0013	-.0014	.0155
-4.96	4.26	.2174	.0192	.0107	.0038	-.0013	.0165
-4.92	6.28	.2906	.0276	.0121	.0054	-.0011	.0175
-4.88	8.37	.3642	.0401	.0150	.0070	-.0007	.0182
-4.82	10.32	.4386	.0565	.0182	.0093	-.0012	.0155
-4.76	12.48	.5206	.0820	.0239	.0099	-.0005	.0141
-4.69	14.80	.6202	.1211	.0350	.0068	.0005	.0085
-5.03	.17	.0660	.0139	.0073	-.0012	-.0011	.0157

TABLE B2.- Concluded

NASA LANGLEY 7 X 10 HIGH SPEED TUNNEL

TEST 59 RUN 33

BETA	ALPHA	CL	CD	CM	CRM	CYM	CY
-5.03	.20	.0713	.0143	.0066	-.0002	-.0004	.0142
-5.09	-5.69	-.1583	.0332	-.0099	-.0039	.0011	.0207
-5.08	-3.74	-.0832	.0226	-.0014	-.0025	.0013	.0171
-5.05	-1.71	-.0035	.0163	.0046	-.0008	.0005	.0150
-5.03	.20	.0711	.0141	.0070	-.0005	-.0006	.0149
-5.00	2.30	.1527	.0154	.0076	.0024	-.0007	.0135
-4.96	4.29	.2236	.0201	.0094	.0049	-.0008	.0152
-4.92	6.35	.2978	.0286	.0110	.0061	-.0006	.0158
-4.88	8.41	.3754	.0415	.0141	.0077	-.0002	.0171
-4.82	10.36	.4461	.0580	.0164	.0103	-.0005	.0140
-4.76	12.51	.5278	.0836	.0225	.0101	.0002	.0129
-4.69	14.82	.6275	.1234	.0332	.0074	.0007	.0079
-5.03	.22	.0729	.0142	.0066	-.0003	-.0004	.0146

TEST 59 RUN 34

BETA	ALPHA	CL	CD	CM	CRM	CYM	CY
4.90	.10	.0694	.0137	.0083	.0015	.0007	-.0145
4.93	-5.81	-.1642	.0337	-.0096	.0045	-.0009	-.0196
4.92	-3.84	-.0868	.0230	-.0003	.0033	-.0011	-.0169
4.92	-1.81	-.0064	.0164	.0054	.0020	-.0005	-.0149
4.90	.14	.0722	.0139	.0087	.0017	.0009	-.0147
4.88	2.18	.1510	.0151	.0092	-.0016	.0008	-.0139
4.86	4.20	.2222	.0194	.0101	-.0042	.0006	-.0138
4.83	6.24	.2984	.0274	.0116	-.0055	.0014	-.0152
4.80	8.30	.3691	.0394	.0138	-.0078	.0013	-.0143
4.76	10.26	.4437	.0573	.0169	-.0089	.0010	-.0125
4.71	12.39	.5247	.0836	.0245	-.0097	-.0003	-.0099
4.64	14.63	.6165	.1195	.0369	-.0122	-.0013	.0021
4.90	.08	.0691	.0139	.0080	.0016	.0008	-.0146

TEST 59 RUN 35

BETA	ALPHA	CL	CD	CM	CRM	CYM	CY
-.08	.05	.0677	.0137	.0086	.0005	.0001	.0016
-.10	-5.81	-.1663	.0340	-.0067	-.0004	.0005	.0019
-.09	-3.86	-.0907	.0231	.0021	.0003	.0004	.0020
-.09	-1.85	-.0093	.0165	.0076	.0005	.0004	.0016
-.08	.09	.0697	.0137	.0087	.0009	.0001	.0017
-.07	2.14	.1520	.0148	.0072	.0008	.0000	.0016
-.07	4.14	.2234	.0194	.0091	.0008	.0000	.0023
-.06	6.18	.2948	.0274	.0109	.0008	.0001	.0030
-.05	8.24	.3745	.0407	.0121	.0012	.0005	.0031
-.06	10.16	.4419	.0558	.0164	-.0001	.0013	.0075
-.05	12.29	.5190	.0766	.0221	.0005	.0006	.0073
-.03	14.59	.6077	.1141	.0328	.0017	-.0004	.0054
-.08	.05	.0677	.0138	.0087	.0007	.0001	.0017

TEST 59 RUN 39

BETA	ALPHA	CL	CD	CM	CRM	CYM	CY
-.07	.12	.0676	.0148	.0094	.0005	-.0001	.0015
-.08	-5.77	-.1708	.0355	-.0046	-.0004	.0001	.0020
-.08	-3.82	-.0912	.0241	.0031	.0001	.0002	.0010
-.07	-1.78	-.0058	.0173	.0086	.0004	.0002	.0016
-.07	.13	.0686	.0149	.0093	.0004	.0000	.0018
-.06	2.28	.1545	.0169	.0084	.0006	-.0002	.0023
-.05	4.18	.2218	.0214	.0098	.0008	-.0001	.0026
-.05	6.19	.2908	.0296	.0123	.0011	-.0001	.0033
-.04	8.28	.3717	.0452	.0143	.0012	.0004	.0020
-.04	10.22	.4458	.0639	.0175	.0005	.0010	.0048
-.04	12.34	.5329	.0921	.0252	-.0000	.0017	.0100
-.02	14.67	.6373	.1361	.0345	.0006	-.0001	.0073
-.07	.13	.0744	.0152	.0089	.0005	-.0000	.0023

REFERENCES

1. Robins, A. Warner; Morris, Odell A.; and Harris, Roy V., Jr.: Recent Research Results in the Aerodynamics of Supersonic Vehicles. J. Aircr., vol. 3, no. 6, Nov.-Dec. 1966, pp. 573-577.

2. Robins, A. Warner; Lamb, Milton; and Miller, David S.: Aerodynamic Characteristics at Mach Numbers of 1.5, 1.8, and 2.0 of a Blended Wing-Body Configuration With and Without Integral Canards. NASA TP-1427, 1979.

3. Coe, Paul L., Jr.; McLemore, H. Clyde; and Shivers, James P.: Effects of Upper-Surface Blowing and Thrust Vectoring on Low-Speed Aerodynamic Characteristics of a Large-Scale Supersonic Transport Model. NASA TN D-8296, 1976.

4. Coe, Paul L., Jr.; Smith, Paul M.; and Parlett, Lysle P.: Low-Speed Wind Tunnel Investigation of an Advanced Supersonic Cruise Arrow-Wing Configuration. NASA TM-74043, 1977.

5. Coe, Paul L., Jr.; and Weston, Robert P.: Effects of Wing Leading-Edge Deflection on Low-Speed Aerodynamic Characteristics of a Low-Aspect-Ratio Highly Swept Arrow-Wing Configuration. NASA TP-1434, 1979.

6. Coe, Paul L., Jr.; and Thomas, James L.: Theoretical and Experimental Investigation of Ground-Induced Effects for a Low-Aspect-Ratio Highly Swept Arrow-Wing Configuration. NASA TP-1508, 1979.

7. Craidon, Charlotte B.: Description of a Digital Computer Program for Airplane Configuration Plots. NASA TM X-2074, 1970.

8. Fox, Charles H., Jr.; and Huffman, Jarrett K.: Calibration and Test Capabilities of the Langley 7- by 10-Foot High Speed Tunnel. NASA TM X-74027, 1977.

9. Gillis, Clarence L.; Polhamus, Edward C.; and Gray, Joseph L., Jr.: Charts for Determining Jet-Boundary Corrections for Complete Models in 7- by 10-Foot Closed Rectangular Wind Tunnels. NACA WROL-123, 1945. (Formerly NACA ARR L5G31.)

10. Pope, Alan; and Harper, John J.: Low-Speed Wind Tunnel Testing, John Wiley & Sons, Inc., c.1966.

11. Braslow, Albert L.; and Knox, Eugene C.: Simplified Method for Determination of Critical Height of Distributed Roughness Particles for Boundary-Layer Transition at Mach Numbers From 0 to 5. NACA TN-4363, 1958.

12. Lamar, John E.; and Gloss, Blair B.: Subsonic Aerodynamic Characteristics of Interacting Lifting Surfaces With Separated Flow Around Sharp Edges Predicted by a Vortex-Lattice Method. NASA TN D-7921, 1975.

13. Polhamus, Edward C.: A Concept of the Vortex Lift of Sharp-Edge Delta Wings Based on a Leading-Edge-Suction Analogy. NASA TN D-3767, 1966.

14. Henderson, William P.: Studies of Various Factors Affecting Drag Due to Lift at Subsonic Speeds. NASA TN D-3584, 1966.

15. Tulinius, J.: Unified Subsonic, Transonic, and Supersonic NAR Vortex Lattice. TFD-72-523, Los Angeles Div., North American Rockwell, Apr. 27, 1972.

16. Grantham, William D.; Nguyen, Luat T.; Deal, Perry L.; Neubauer, M.J., Jr.; Smith, Paul M.; and Gregory, Frederick D.: Ground-Based and In-Flight Simulator Studies of Low-Speed Handling Characteristics of Two Supersonic Cruise Transport Concepts. NASA TP-1240. 1978.

17. Coe, Paul L.; Jr.; and Gilbert, William P.: Application of Low-Speed Aerodynamic Characteristics of Highly Swept Arrow-Wing Configurations to Supersonic Cruise Tactical Fighter Designs. Design Conference Proceedings - Technology for Supersonic Cruise Military Aircraft, Volume I, AFFDL-TR-77-85, Vol. I, U.S. Air Force, 1976.

18. Etkin, Bernard: Dynamics of Flight. John Wiley & Sons, Inc., c.1959.

19. Grafton, Sue B.; Chambers, Joseph R.; and Coe, Paul L., Jr.: Wind-Tunnel Free-Flight Investigation of a Model of a Spin-Resistant Fighter Configuration. NASA TN D-7716, 1974.

20. Ribner, Herbert S.: The Stability Derivatives of Low-Aspect-Ratio Triangular Wings at Subsonic and Supersonic Speeds. NACA TN 1423, 1947.

21. Campbell, John P.; and McKinney, Marion O.: Summary of Methods for Calculating Dynamic Lateral Stability and Response and for Estimating Lateral Stability Derivatives. NACA Rep. 1098, 1952. (Supersedes NACA TN 2409.)

1. Report No.	2. Government Accession No.	3. Recipient's Catalog No.
NASA TP-1777		

4. Title and Subtitle	5. Report Date
LEADING-EDGE DEFLECTION OPTIMIZATION FOR A HIGHLY SWEPT ARROW-WING CONFIGURATION	December 1980
	6. Performing Organization Code 533-01-43-02
7. Author(s) Paul L. Coe, Jr., Jarrett K. Huffman, and James W. Fenbert	8. Performing Organization Report No. L-13820
	10. Work Unit No.
9. Performing Organization Name and Address NASA Langley Research Center Hampton, VA 23665	11. Contract or Grant No.
	13. Type of Report and Period Covered Technical Paper
12. Sponsoring Agency Name and Address National Aeronautics and Space Administration Washington, DC 20546	14. Sponsoring Agency Code

15. Supplementary Notes

16. Abstract

An experimental investigation has been conducted to determine the influence of an optimized leading-edge deflection on the low-speed aerodynamic performance of a configuration with a low-aspect-ratio, highly swept wing. Tests have also been conducted to determine the sensitivity of the lateral-stability derivative C_{l_β} to geometric anhedral.

The optimized leading-edge deflection was developed by aligning the leading edge with the incoming flow along the entire span. Owing to the spanwise variation of upwash, the resulting optimized leading edge was a smooth, continuously warped surface. For the particular configuration studied, levels of leading-edge suction on the order of 90 percent were achieved with the smooth, continuously warped leading-edge contour. The results of tests conducted to determine the sensitivity of C_{l_β} to geometric anhedral indicate values of $\partial C_{l_\beta}/\partial \Gamma$ which are in reasonable agreement with estimates provided by simple vortex-lattice theories.

17. Key Words (Suggested by Author(s))	18. Distribution Statement
Arrow wing Leading-edge deflection Subsonic performance	Unclassified - Unlimited Subject Category 02

19. Security Classif. (of this report)	20. Security Classif. (of this page)	21. No. of Pages	22. Price
Unclassified	Unclassified	56	A04

For sale by the National Technical Information Service, Springfield, Virginia 22161

NASA-Langley, 1980